Static and Dynamic Critical Behavior of a Symmetrical Binary Fluid: A Computer Simulation

Subir K. Das,[1] Jürgen Horbach,[2] Kurt Binder,[2] Michael E. Fisher,[1] and Jan V. Sengers[1]

[1] *Institute for Physical Science and Technology, University of Maryland, College Park, MD 20742, USA*

[2] *Institut für Physik, Johannes Gutenberg Universität Mainz, Staudinger Weg 7, 55099 Mainz, Germany*

(Dated: February 6, 2008)

Abstract

A symmetrical binary, A+B Lennard-Jones mixture is studied by a combination of semi-grandcanonical Monte Carlo (SGMC) and Molecular Dynamics (MD) methods near a liquid-liquid critical temperature T_c. Choosing equal chemical potentials for the two species, the SGMC switches identities (A $\rightarrow$ B $\rightarrow$ A) to generate well-equilibrated configurations of the system on the coexistence curve for $T < T_c$ and at the critical concentration, $x_c = 1/2$, for $T > T_c$. A finite-size scaling analysis of the concentration susceptibility above T_c and of the order parameter below T_c is performed, varying the number of particles from $N = 400$ to 12800. The data are fully compatible with the expected critical exponents of the three-dimensional Ising universality class.

The equilibrium configurations from the SGMC runs are used as initial states for microcanonical MD runs, from which transport coefficients are extracted. Self-diffusion coefficients are obtained from the Einstein relation, while the interdiffusion coefficient and the shear viscosity are estimated from Green-Kubo expressions. As expected, the self-diffusion constant does not display a detectable critical anomaly. With appropriate finite-size scaling analysis, we show that the simulation data for the shear viscosity and the mutual diffusion constant are quite consistent both with the theoretically predicted behavior, including the critical exponents and amplitudes, and with the most accurate experimental evidence.

PACS numbers: 47.27.ek, 64.60.Fr, 66.10.Cb, 64.60.Ht

I. INTRODUCTION

Recently, there has been a renewed interest in the critical behavior of simple and complex fluids, both with respect to liquid-gas transitions and demixing transitions in binary fluids.[1,2,3,4,5,6,7,8,9,10] There has been remarkable progress both in the fuller theoretical understanding of the asymptotic critical region and the types of correction to scaling that occur in these systems,[1] and of the nature of the crossover towards classical, van der Waals-like behavior further away from the critical point.[2] Also, the values of the critical exponents and other universal properties (such as critical amplitude ratios) are now known with high precision, from a variety of techniques (renormalization group,[3] Monte Carlo simulations,[4,5] and high-temperature series expansions[6]). Particularly relevant in the present context are advances in the finite-size scaling analysis of computer simulations of fluids,[7,8,9,10] which allow one to study both universal and non-universal critical properties of various off-lattice models of fluids with an accuracy that is competitive with the work on Ising lattice models.[4,5]

With respect to critical dynamics in fluids, the situation is much less satisfactory even though precise experimental data were presented a long time ago[11] and theoretical analyses invoking either approximations, such as mode coupling theory[12,13,14,15,16,17] or low-order renormalization group expansions in $\epsilon = 4 - d$, where d is the dimensionality,[18,19,20,21] do exist. One should note that dynamic universality classes encompass fewer systems than static ones:[19,20] while uniaxial ferromagnets, binary alloys, liquid-gas criticality and demixing in binary fluids all belong to the same universality class as far as their static critical behavior is concerned, these systems belong to more than one dynamic universality class. Thus, there is a clear need for more theoretical analyses of critical dynamics.

Particularly scarce are simulations of the critical dynamics of fluids: of recent works, we are aware only of a nonequilibrium Molecular Dynamics (NEMD) calculation for a two-dimensional fluid in which heat conduction near the critical point was studied,[22] and of a similar investigation by Chen *et al.*[23] of a three-dimensional Lennard-Jones single component fluid. Beyond that Jagannathan and Yethiraj (JY)[24] used a three-dimensional Widom-Rowlinson model[25] to study the inter-diffusional critical dynamics in a binary-fluid. However, the conclusions of this latter work have been seriously challenged.[23,26]

In the present paper, we move to fill this gap by presenting a comprehensive simulation study of critical dynamics in fluids by studying a symmetric binary fluid Lennard-Jones

mixture. In previous work[27,28,29] we have shown that the coexistence curve, concentration susceptibility, interfacial tension between coexisting liquid phases, pair correlation functions and static and dynamic structure factors for this model can be reliably estimated *via* a combination of semi-grandcanonical Monte Carlo methods (SGMC)[27,28,29,30,31,32,33,34] and microcanonical Molecular Dynamics (MD) methods.[35,36,37,38] Transport coefficients such as self-diffusion and interdiffusion coefficients,[27] shear viscosity[27] and bulk viscosity[28] were estimated *away* from the critical region. Here, however, we expressly address the critical behavior of the model and compare with theoretical expectations. Moreover, our study strongly supports the challenge[26] to the earlier study by JY[24] of the somewhat similar but less realistic Widom-Rowlinson model.

In the balance of this article, Section II presents the model and briefly reviews our simulation methods. Section III discusses the static critical properties that are extracted from the "raw data" by a finite-size scaling analysis.[39,40,41,42] Sec. IV then presents our results on the selfdiffusion coefficients and the shear viscosity: we discuss them in the light of the theoretical predictions.[12,13,14,15,16,17,18,19,20,21] The interdiffusional coefficient, which vanishes fairly strongly, requires more detailed, specifically, finite-size scaling considerations, etc. which are presented in Sec. V. The article concludes in Sec. VI with a brief summary and discussion.

II. MODEL AND SIMULATION TECHNIQUES

Following Refs. $27-29$ we consider a binary fluid of point particles with pairwise interactions in a cubical box of finite volume $V = L^3$ subject to periodic boundary conditions. Starting from a full Lennard-Jones potential

$$\Phi_{\rm LJ}(r_{ij}) = 4\varepsilon_{\alpha\beta}[(\sigma_{\alpha\beta}/r_{ij})^{12} - (\sigma_{\alpha\beta}/r_{ij})^{6}] \,, \tag{1}$$

we construct a truncated potential that is strictly zero for $r_{ij} \geq r_c$ as follows,[35]

$$u(r_{ij}) = \Phi_{\rm LJ}(r_{ij}) - \Phi_{\rm LJ}(r_c) - (r_{ij} - r_c)\frac{d\Phi_{\rm LJ}}{dr_{ij}}|_{r_{ij}=r_c}, \text{ for } r_{ij} \leq r_c. \tag{2}$$

This form ensures that both the potential and the force are continuous at $r = r_c$. In the previous work,[27,28,29] the last term on the right-hand-side of Eq. (2) was not included so that the force at $r_{ij} = r_c$ exhibited a jump, while only the potential was continuous. This is not

desirable when considering dynamic behavior, because, in a microcanonical simulation, this results in a drift of the total energy.

The parameters in Eqs. (1) and (2) were chosen as

$$\sigma_{\rm AA} = \sigma_{\rm BB} = \sigma_{\rm AB} = \sigma \ , \tag{3}$$

and, hence, we adopt σ as our unit of length. The cutoff r_c is chosen as $r_c = 2.5\sigma$. As previously,[27,28,29] we take the total particle number $N = N_{\rm A}+N_{\rm B}$ of the binary A+B mixture and the volume such that the density $\rho^* = \rho\sigma^3 = N\sigma^3/V = 1$. This choice is convenient, since the system is then in its liquid (rather than its vapor) phase and crystallization is not yet a problem at the temperatures of interest. Finally, the reduced temperature T^* and energy parameters $\varepsilon_{\alpha\beta}$ are chosen as[27,28,29]

$$T^* = k_{\rm B}T/\varepsilon \quad \text{and} \quad \varepsilon_{\rm AA} = \varepsilon_{\rm BB} = 2\varepsilon_{\rm AB} = \varepsilon. \tag{4}$$

The system is equilibrated as follows. First, a Monte Carlo (MC) run is performed in the canonical ensemble ($N_{\rm A}$=$N_{\rm B}, V, T$), starting out from particles at random positions in the simulation box. The MC moves used are random displacements of randomly chosen single particles (selecting the trial value of each new cartesian coordinate in the range $[-\sigma/20, +\sigma/20]$ about its old value) and applying the standard Metropolis acceptance criterion.[31,32] These initial runs were carried out for 10^4 Monte Carlo steps (MCS) per particle, for systems with particle numbers from $N = 400$ to $N = 12800$. Then equilibration is continued, using the semi-grandcanonical Monte Carlo (SGMC) method.[27,28,29,30,31,32,33,34] After 10 displacement steps per particle $N/10$ particles are randomly chosen in succession and an attempted identity switch is made, A $\to$ B or B $\to$ A, where both the energy change, ΔE, and the chemical potential difference, $\Delta\mu$, between A and B particles enters the Boltzmann factor. However, we restrict attention here to the special case $\Delta\mu = 0$, which, for the symmetric mixture considered, means that for $T > T_c$ we simulate states with an average concentration $\langle x_{\rm A}\rangle = \langle x_{\rm B}\rangle = 1/2$ (with $x_\alpha = N_\alpha/N$), while for $T < T_c$ we simulate states along either the A-rich or the B-rich branch of the coexistence curve.

In the semi-grandcanonical ensemble, the concentration $x_{\rm A}$ is a fluctuating variable, and hence the probability distribution $P(x_{\rm A})$ can be recorded: this is particularly useful in the context of a finite-size scaling analysis.[39,40,41,42] In addition, use of the semi-grandcanoncial ensemble for the study of static critical properties in a binary fluid mixture is preferable

since critical slowing down is somewhat less severe than in the canonical ensemble. Critical slowing down limits the accuracy that can be attained, since the statistical error scales like $1/\sqrt{n}$, where n is the number of statistically independent configurations.[34] The statistically independent configurations used in the computation of averages must be separated from each other along the stochastic (MC) or deterministic (MD) trajectory of the simulation by a time interval which is of order of the longest relaxation time in the system.[34] In a finite system at the demixing critical point of a fluid binary mixture, this slowest relaxation time scales with box dimension L as

$$\tau_{max} \propto L^z, \tag{5}$$

where z is a universal dynamic critical exponent, which depends on the dynamic universality class.[18,19,20,21] For the SGMC algorithm, the order parameter (concentration difference between A and B) is not a conserved variable, while the average density $\rho = N/V$ is conserved. As a consequence, this model belongs to "class C" in the Hohenberg-Halperin classification,[19] and hence the dynamic exponent is roughly $z = 2$.[18,19] If we performed MC simulations in the $N_{\rm A}N_{\rm B}VT$ ensemble, the order parameter would be a conserved variable, in addition to the density ("class D"[19]), and then the dynamic critical exponent is expected to be significantly larger, $z = 4 - \eta$, where η ($\simeq 0.03$)[3,4,5] describes the spatial decay of correlations at criticality. If one performs MD runs in a microcanonical $N_{\rm A}N_{\rm B}VE$ ensemble (with $N_{\rm A} = N_{\rm B}$ and with an energy chosen so that the system is precisely at the critical point), the dynamic exponent is predicted to be $z \simeq 3$.[16,17,18] In fact, Jagannathan and Yethiraj[24] used Eq. (5) in order to explore the critical dynamics of their Widom-Rowlinson model.[25] Comparing the values of z for the three algorithms discussed above, it is clear why the SGMC algorithm has an advantage, as far as static critical properties are concerned.

For the study of dynamic critical properties, multiple independent initial configurations were prepared,[43] from SGMC runs with 5×10^5 MCS (but excluding states from the first 10^5 MCS). Then a further thermalization for 2×10^5 MD steps was carried out in the NVT ensemble using the Andersen thermostat.[35,36,37,38] For all MD runs, we always chose the masses of the particles equal to each other, $m_{\rm A} = m_{\rm B} = m$, and applied the standard velocity Verlet algorithm[35,36,37,38] with a time step $\delta t^* = 0.01/\sqrt{48}$ where $t^* = t/t_0$ with scale factor

$$t_0 = (m\sigma^2/\varepsilon)^{1/2}. \tag{6}$$

The final production runs in the microcanonical ensemble (where the Andersen thermostat is switched off) used from about 10^6 MD steps for temperatures $T^* = 1.5$ and higher, but up to 2.8×10^6 MD steps for T close to T_c (where $T_c^* = 1.4230 \pm 0.0005$, see below). To avoid confusion, we note that the different value of T_c in the previous work,[27,28,29] namely, $T_c^* = 1.638 \pm 0.005$, arose from the different choice of potential (the last term on the right hand side of Eq. (2) being absent in Refs. $27-29$).

III. STATIC CRITICAL PROPERTIES

Using the SGMC algorithm we record the fluctuating number of A particles $N_{\rm A}$ (recall that $N_{\rm B} = N - N_{\rm A}$ with the total particle number N fixed) and generate histograms to estimate the probability distribution $P(x_{\rm A})$ of the relative concentration $x_{\rm A} = N_{\rm A}/N$. Typical "raw data" for $P(x_{\rm A})$ are shown in Fig. 1. The symmetry relation that holds for $\Delta\mu = 0$, namely,

$$P(x_{\rm A}) = P(1 - x_{\rm A}), \tag{7}$$

has been incorporated in the data. This has been done because below T_c, where $P(x_{\rm A})$ has a pronounced double-peak structure corresponding to the two sides $x_{\rm A}^{\rm coex(1)}$, $x_{\rm A}^{\rm coex(2)}$ of the two-phase coexistence curve, transitions from one side to the other occur very infrequently (or, at low temperatures, not at all). In Fig. 1(a) we present probability distributions for several temperatures below T_c while Fig. 1(b) shows the distributions for temperatures above T_c. From $P(x_{\rm A})$, we define the truncated moments $\langle x_{\rm A}^k \rangle$ of the concentration distribution as follows[27]

$$\langle x_{\rm A} \rangle = 2 \int_{1/2}^{1} x_{\rm A} P(x_{\rm A}) dx_{\rm A} \ , \tag{8}$$

$$\langle x_{\rm A}^k \rangle = 2 \int_{1/2}^{1} x_{\rm A}^k P(x_{\rm A}) dx_{\rm A} \ . \tag{9}$$

The two branches of the coexistence curve can then be estimated for large N via

$$x_{\rm A}^{\rm coex(1)} \simeq (1 - \langle x_{\rm A} \rangle), \quad x_{\rm A}^{\rm coex(2)} \simeq \langle x_{\rm A} \rangle \ , \tag{10}$$

while the "concentration susceptibility" χ and its dimensionless form, χ^*, can be estimated from

$$k_{\rm B} T \chi = T^* \chi^* = N(\langle x_{\rm A}^2 \rangle - 1/4), \quad T > T_c. \tag{11}$$

Another useful quantity is the fourth-order cumulant U_L, defined by[4,40,44]

$$U_L(T) = \langle (x_{\rm A} - 1/2)^4 \rangle / [\langle (x_{\rm A} - 1/2)^2 \rangle^2]. \tag{12}$$

Note that for a finite system, $(\langle x_A \rangle - 1/2)$ remains nonzero even for $T \geq T_c$ [as seen in Fig. 1(b)]. Furthermore $\langle x_A \rangle$ is a smooth function of temperature for finite L while χ likewise remains finite at T_c. Due to these effects, a finite-size scaling analysis of the SGMC data for these quantities is clearly required, as is well known.[34,40,42]

There are different strategies used in the literature to estimate the location of the critical temperature T_c from such simulation results.[4,5,7,8,9,10,34,37,40,42] The simplest method, most often used for fluids, records $x_{\rm A}^{\rm coex(1)}, x_{\rm A}^{\rm coex(2)}$ for several choices of L and checks for a regime of temperatures below T_c where the results are independent of L within statistical errors. In this regime one chooses several temperatures, as close to T_c as possible, and fits to a power law

$$x_{\rm A}^{\rm coex(2)} - x_{\rm A}^{\rm coex(1)} = B(1 - T/T_c)^{\beta} \, , \tag{13}$$

where the critical amplitude B and T_c are adjustable parameters, while the critical exponent β is fixed at its theoretical value for the universality class of the three-dimensional Ising model, $\beta \simeq 0.325$.[3,4,5,6]

In Fig. 2, we show the two-phase coexistence curve for $N = 6400$. (Recall that for our choice we have density $\rho^* = 1$, so the system size is $L = N^{1/3}\sigma$.) The dashed line in Fig. 2 is a guide to the eye for the numerical data (open circles). The continuous line is a fit to Eq. (13) using the range from $0.2 < x_{\rm A} < 0.5$ (but excluding the two points closest to T_c). From this we obtain $T_c^* = 1.423 \pm 0.002$ and $B = 1.53 \pm 0.05$. This fit is good over a relatively wide range of temperature but, in reality, the range over which Eq. (13) should be valid is significantly smaller owing to various corrections to scaling[3,4,5,6] which have been neglected. Hence, systematic uncontrollable errors easily arise: the true value of T_c could well be somewhat lower with B larger. Alternative methods are thus needed to obtain more reliable estimates of T_c with improved error bounds. Indeed one clear drawback of the previous study on critical dynamics by JY[24] is that the accuracy with which the critical point could be located was relatively poor.

A method used more recently in Monte Carlo studies of critical phenomena[37,40,42] is data collapsing based on the finite-size scaling hypothesis.[39,42] Let us consider the concentration susceptibility χ in the vicinity of the critical point. At the critical concentration, $x_A = x_B =$

1/2, we have

$$\chi^*(T) \approx \Gamma_0 \epsilon^{-\gamma} \quad \text{with} \quad \epsilon = (T - T_c)/T_c, \tag{14}$$

where Γ_0 and γ are the critical amplitude and critical exponent, respectively. From here on we shall use the symbol ϵ for the reduced temperature deviation to avoid confusion with t which arises naturally as a symbol for time in the context of MD simulations. For a system of finite size L, the basic scaling ansatz may be written as

$$\chi_L^*(T) \approx \Gamma_0 Z(y) \epsilon^{-\gamma}, \tag{15}$$

where $y = L/\xi$, in which ξ is the correlation length, while $Z(y)$ is the appropriate finite-size scaling function. The correlation length diverges at criticality as

$$\xi \approx \xi_0 \epsilon^{-\nu}, \tag{16}$$

with amplitude ξ_0 and exponent ν. In the limit $y \to \infty$ (so that $L \to \infty$ at fixed $\epsilon > 0$) the scaling function $Z(y)$ must approach unity so that Eq. (14) is recovered. For static quantities (such as χ), in short-range systems with periodic boundary conditions, $Z(y)$ generally approaches unity exponentially fast. So, one may expect the behavior

$$Z(y) = 1 + Z_\infty y^\psi e^{-ny} + ..., \quad \text{for} \quad y \to \infty, \tag{17}$$

where the values of the exponent ψ and the integer $n = 1, 2, 3, ...$ depend upon the details of the system in question. On the other hand, for finite L, in the limit $y \to 0$ (so $\epsilon \to 0$ at fixed $L < \infty$), the susceptibility $\chi_L(T)$ is finite and its variation with T must be smooth and analytic. Thus one should have

$$Z(y) = y^{\gamma/\nu}[Z_0 + Z_1 y^{1/\nu} + Z_2 y^{2/\nu} + ... \,] \quad \text{as} \quad y \to 0. \tag{18}$$

An effective procedure is then to study the computed quantity $\chi_L^*(T)\epsilon^\gamma$ as a function of y for different system sizes by using T_c as an adjustable parameter to optimize the data collapse. The plot should then approach $\Gamma_0 Z(y)$. From the asymptotic behavior of $\Gamma_0 Z(y)$ as y becomes large one can then estimate the critical amplitude. In Fig. 3 we plot $\chi_L^*(T)\epsilon^\gamma$ vs. $y/(y + y_0)$ noting that the abscissa variable approaches zero when $y \to 0$ but tends to unity when $y \to \infty$ for $y_0 > 0$. For convenience we have chosen $y_0 = 7$ which is comparable with the value of L/ξ for the largest system size. (This point will be discussed further.) Of course, if one wishes to estimate all three quantities T_c, γ and ν from such a procedure, one again

fights hard to control systematic errors since the uncertainities in the estimates for these quantities are inevitably highly correlated. Accordingly we have fixed the critical exponents at their universal values, accurately known from other studies,[3,4,5,6] $\gamma \simeq 1.239, \nu \simeq 0.629$, since there is no reason to doubt that these exponents describe the static critical behavior of the present model.

In Fig 3, we demonstrate data collapse for four trial values of T_c. It is clear that the collapse is inferior for the values $T_c^* = 1.425$ and 1.419 compared to the choices 1.423 and 1.421: the collapse looks quite acceptable in these latter cases. Thus, we conclude that our previous estimation of T_c is consistent with this analysis.

An unbiased method to evaluate T_c utilizes the fourth-order cumulant defined in Eq.(12):[40,44] plotting $U_L(T)$ vs. T for various sizes L one finds T_c from a common intersection point of these curves once corrections to finite-size scaling become negligible. Quite generally one has $U_L \to 1/3$ in any one-phase region while $U_L \to 1$ on the coexistence-curve diameter in the two-phase region. Furthermore, for the three-dimensional Ising universality class $U_L(T_c)$ takes the value 0.6236.[8,9]

In Fig. 4(a) we present $U_L(T)$ for several system sizes (as indicated in the figure) over a rather wide range of temperature. The horizontal dashed line indicates the value of this quantity at the critical point for the Ising universality class. This plot clearly confirms that our model belongs to the three-dimensional Ising universality class. While on a coarse scale the expected intersection is nicely seen, the enlarged view of the data, in Fig 4(b), reveals some scatter, which is mainly due to the statistical errors of the simulation data [as can be seen, by comparing with plots in Refs. 8, 9(c) and 45]. In light of these statistical errors, further analyses are clearly not warranted. Thus, for example, the method of Wilding[7] based on the use of the full distribution $P(x_A)$ at criticality, rather than using only the second and fourth moment, is not tried here: but see also the critique in Ref. 46. In Fig. 4(b), the smooth lines are fits to the hyperbolic tangent function. For the system sizes shown, these fits all intersect one another close to $T^* = 1.423$ and at the Ising critical value[4] 0.6236. Since this method appears to be the most reliable currently available in the literature, we adopt

$$T_c^* = 1.4230 \pm 0.0005 \tag{19}$$

for the subsequent analysis of our simulation data.

Of course, it is also of interest to extract the pair correlation functions $g_{\rm AA}(r)$, $g_{\rm AB}(r)$

and $g_{\rm BB}(r)$ and their Fourier transforms, $S_{\rm AA}(q)$, $S_{\rm AB}(q)$ and $S_{\rm BB}(q)$, as described for a closely related model (outside the critical region) in earlier work.[27] Of particular interest are the combinations that single out number-density fluctuations $S_{nn}(q)$ and concentration fluctuations $S_{cc}(q)$, defined via[47]

$$S_{nn}(q) = S_{\rm AA}(q) + 2S_{\rm AB}(q) + S_{\rm BB}(q) \ , \tag{20}$$

$$S_{cc}(q) = (1-x_{\rm A})^2 S_{\rm AA}(q) + x_{\rm A}^2 S_{\rm BB}(q) - 2x_{\rm A}(1-x_{\rm A})S_{\rm AB}(q) \ . \tag{21}$$

Fig. 5(a) shows that $S_{nn}(q)$ exhibits the normal oscillatory behavior of the structure factor of a dense liquid: the approach to criticality has little discernible effect. By contrast, $S_{cc}(q)$ varies weakly at large q, corresponding to small spatial length scales, while at small q a strong increase is observed. Of course, this is the expected Ornstein-Zernike behavior reflecting the "critical opalescence" due to concentration fluctuations: see Fig. 5(b). The inset here displays an Ornstein-Zernike plot, based on

$$S_{cc}(q) = k_{\rm B}T\chi/[1 + q^2\xi^2 + ...], \tag{22}$$

from which our estimates of the correlation length ξ have been extracted. Note that, in the fitting process, we have used the value of $k_{\rm B}T\chi$ from our SGMC simulations.

In Fig. 6 we plot the susceptibility and correlation length $\chi^*(T)$ and $\xi(T)$, as functions of ϵ for $N = 6400$ and fit the data with the respective asymptotic forms (14) and (16). For the fitting we again adopt the Ising critical exponent values, so that the amplitudes are the only adjustable parameters. The quality of the fits suggests that the finite-size effects are negligible in this temperature range (where as one sees from Fig. 3, $y \gtrsim 4$ so that $L \gtrsim 4\xi(T)$). The amplitudes are found to be

$$\xi_0/\sigma = 0.395 \pm 0.025, \quad \Gamma_0 = 0.076 \pm 0.006. \tag{23}$$

In Fig. 6(c) we plot χ vs. ξ. The continuous line is a power-law fit with the exponent $\gamma/\nu \simeq 1.970$.

We conclude this section by noting that no unexpected features have been uncovered. The static properties comply fully with the anticipated critical behavior characterizing three-dimensional Ising-type systems. Furthermore, the corrections to scaling seem to be quite small in the temperature range covered by our simulations, so that one can observe the asymptotic power laws even relatively far from the critical temperature.

IV. SELF-DIFFUSION COEFFICIENT AND SHEAR VISCOSITY NEAR CRITICALITY

The transport coefficients which are most readily found from simulations are the self-diffusion coefficients $D_{\rm A}$ and $D_{\rm B}$ which can be extracted from the Einstein relations for the mean square displacements of tagged particles,[48] namely,

$$g_{\rm A}(t) = \langle [\vec{r}_{i,{\rm A}}(0) - \vec{r}_{i,{\rm A}}(t)]^2 \rangle, \tag{24}$$

and likewise for $g_{\rm B}(t)$, where it is understood that the average $\langle \ldots \rangle$ includes an average over all particles of type A or B, respectively. The self-diffusion coefficients then follow from

$$D^*_{\rm A} = (t_0/\sigma^2) D_{\rm A} = (t_0/\sigma^2) \lim_{t\to\infty} [g_{\rm A}(t)/6t], \tag{25}$$

and similarly for $D_{\rm B}$. In the region above T_c and at critical concentration $x_{\rm A} = x_{\rm B} = 1/2$, to which we will restrict attention, the symmetry of the model requires $g_{\rm A}(t) = g_{\rm B}(t)$ and $D_{\rm A} = D_{\rm B} = D$. To extract D and study its temperature dependence we have hence averaged over the mean square displacements of all particles: see Fig. 7. Note that in the initial, ballistic regime $g_{\rm A}(t)$ varies quadratically with t before crossing over to linear diffusive behavior from which $D_{\rm A}$ is estimated. As expected, the temperature dependence of D is rather weak and, indeed, close to linear over this fairly narrow temperature range; moreover, D appears to remain nonzero at $T = T_c$ with a value close to $D^* = 0.048$. Indeed, there is no sign of any critical anomaly, consistent with the previous work of JY.[24] Similarly, a study of self-diffusion near the vapor-liquid critical point of a lattice gas model[49] did not detect any significant critical anomaly. (Note, however, that this latter model belongs to class B in the Hohenberg-Halperin classification.[19]) Nevertheless, a weak anomalous decrease of the self-diffusion coefficient at the critical density has been seen in simulations of simple fluids near the vapor-liquid critical point,[50] but has not yet been confirmed experimentally.[51]

Next we consider the reduced shear viscosity η^* which we calculate from the Green-Kubo formula[52]

$$\eta^*(T) = (t_0^3/\sigma V m^2 T^*) \int_0^\infty dt \langle \sigma_{xy}(0)\sigma_{xy}(t)\rangle, \tag{26}$$

where the pressure tensor $\sigma_{xy}(t)$ is given by

$$\sigma_{xy}(t) = \sum_{i=1}^{N} [m_i v_{ix} v_{iy} + \frac{1}{2} \sum_{j(\neq i)} |x_i - x_j| F_y(|\vec{r}_i - \vec{r}_j|)], \tag{27}$$

in which $\vec{v}_i$ is the velocity of particle i while $\vec{F}$ is the force acting between particles i, j.

Theory[14,15,16] suggests that at the critical point η^* should diverge as

$$\eta^* \approx \eta_0 \epsilon^{-\nu x_\eta} \sim \xi^{x_\eta}, \tag{28}$$

where η_0 and $x_\eta > 0$ are the appropriate critical amplitude and exponent. Renormalization-group theory[18,19] predicts $x_\eta \simeq 0.065$ while the theory of Ferrell and Bhattacharjee[53] yields $x_\eta \simeq 0.068$. These values are consistent with experiments[54,55] which yield x_η between 0.064 and 0.070. The most recent theoretical estimate is[53] 0.0679 ± 0.0007 and the most recent experimental value is[54] 0.0690 ± 0.0006.

Fig. 8 displays a log-log plot of η^* vs. ϵ. As normal in MD simulations, accurate estimation of the shear viscosity is difficult and the large error bars shown in Fig. 8 prevent us from making definitive statements about the critical singularity. But the slow increase of η^* as $T \to T_c$ is, in fact, compatible with the expected power law divergence, as Fig. 8 shows, since the fitted line has a slope corresponding to $\nu = 0.629$ and $x_\eta = 0.068$ in Eq. (28). Although this fit is consistent with the theoretical prediction, estimating νx_η from the data itself is clearly of little value. However, the amplitude, for which we obtain $\eta_0 = 3.8_7 \pm 0.3$, will prove to be significant.

At this point it is of interest to check the validity of the Stokes-Einstein relation, which relates the self-diffusion constant of a diffusing spherical particle of diameter d to the shear viscosity of the fluid $\eta(T)$. For a particle moving in a fluid of like particles, the Stokes-Einstein diameter d can be written[27]

$$d = \sigma T^* / 2\pi \eta^* D^*, \tag{29}$$

which corresponds to the assumption of slip boundary conditions on the surface of the diffusing sphere. For stick boundary conditions, a factor 3 replaces the factor 2 in Eq. (29). In Fig. 9, we present a plot of d in the interval $T^* = 1.45$ to 1.55. The data suggest that Eq. (29) is still a valid approximation despite the strong concentration fluctuations close to T_c. However, we do not expect the relation to remain valid closer still to T_c since $\eta(T)$ diverges, albeit slowly, while D remains finite.

V. INTERDIFFUSION: FINITE-SIZE SCALING

Finally we consider the interdiffusion or mutual diffusion coefficient, which is expected to vanish at the critical point. Following the previous work[27,28,29] we use the Green-Kubo formula[52] which we express as

$$D_{\rm AB}(T) = \frac{\sigma^2}{t_0} D^*_{\rm AB}(T) = \frac{\sigma^2}{t_0} \lim_{t\to\infty} D^*_{\rm AB}(T;t), \tag{30}$$

where, introducing the appropriate reduced Onsager coefficient,

$$\mathcal{L}(T) = \lim_{t\to\infty} \mathcal{L}(T;t), \tag{31}$$

we have the relation

$$D^*_{\rm AB}(T;t) = \mathcal{L}(T;t)/\chi^*(T), \tag{32}$$

in which, for numerical purposes, we will use our fits to Eq. (14) for χ^*, while

$$\mathcal{L}(T;t) = (t_0/N\sigma^2 T^*) \int_0^t dt' \langle J_x^{\rm AB}(0) J_x^{\rm AB}(t')\rangle, \tag{33}$$

in which the current vector $\vec{J}^{\rm AB}$ is defined by

$$\vec{J}^{\rm AB}(t) = x_{\rm B} \sum_{i=1}^{N_{\rm A}} \vec{v}_{i,{\rm A}}(t) - x_{\rm A} \sum_{i=1}^{N_{\rm B}} \vec{v}_{i,{\rm B}}(t) \ , \tag{34}$$

where $\vec{v}_{i,\alpha}(t)$ denotes the velocity of particle i of type α at time t.

Since the correlation function $\langle J_x^{\rm AB}(0) J_x^{\rm AB}(t)\rangle$ is rather noisy at large times comparable to the total observation time, $t_{\rm obs}$, of an MD run, it is difficult to attain a precision for $D_{\rm AB}$ as high as for the self-diffusion constant D. This problem is evident in Fig. 10, where short-time maxima (seen for $t^* \simeq 0.1$) are followed by shallow minima (at $t^* \simeq 0.5 - 0.6$) that appear before the expected plateau starts at about $t^* \simeq 4$. For times $t^* \geq 40$, the curves become progressively more noisy, and, clearly, at most temperatures the data for $t^* \geq 100$ may be discarded owing to deficient statistics. But, in any case, the facts that the general shape of the curves is similar for all temperatures studied, and, in particular, that the time needed for $D_{\rm AB}(t)$ to reach a plateau value is almost independent of T, suggest that the dominant contribution to the temperature dependence of $D_{\rm AB}$ arises from χ^* in Eq. (32).

Fig. 11 presents plots of $D^*_{\rm AB}(T)$ versus T for systems of $N = 6400$ particles. One sees that $D_{\rm AB}$ has the apparent power-law behavior

$$D_{\rm AB} \sim \xi^{-x_{\rm eff}} \sim \epsilon^{x_{\rm eff}\nu} \simeq \epsilon^1, \quad \text{with} \quad x_{\rm eff}\nu \simeq 1, \quad \text{so} \quad x_{\rm eff} \simeq 1.6. \tag{35}$$

This result is in strong disagreement with the theoretical prediction for the interdiffusional critical exponent,[53] namely,

$$x_D = 1 + x_\eta \simeq 1.0679, \tag{36}$$

that should be accessible asymptotically when $T \to T_c$. Indeed, the value of $x_{\rm eff}$ found from Fig. 11 is even larger than the value $x_D = 1.26 \pm 0.08$ quoted by JY[24] for their binary fluid model. However, it would be quite erroneous to conclude from our data and Fig. 11 that the simulations indicate a serious failure of the theory. Even though we have found that the finite-size effects in the equilibrium *static* properties are small for the temperature range and system sizes explored [where $L \gtrsim 4\xi(T)$], one must be prepared to encounter much stronger finite-size corrections in *transport* properties near criticality.

In addition experiments have shown that the Onsager coefficient near a liquid-liquid demixing critical point or its equivalent, the thermal conductivity near a vapor-liquid critical point, may have a significant noncritical background contribution arising from short-range fluctuations.[56,57]

Thus it is crucial to analyze dynamical simulations by making proper allowance for the finite-size behavior and also for possibly significant 'background' contributions to the quantities computed.[58] To this end we consider, as above, only the critical isopleth $x_{\rm A} = x_{\rm B} = 1/2$ and will focus on the finite-size Onsager coefficient $\mathcal{L}_L(T)$ as defined via Eq. (33). The prime reason for analyzing the Onsager coefficient rather than the interdiffusional constant $D_{\rm AB}(T)$ (which clearly follows by dividing by χ) is that it represents most directly the basic fluctuation sum/integral analogous to expressions like Eq. (11) defining χ, or the standard fluctuation sums for the specific heat, etc.;[52] experience teaches that such properties display the simplest, albeit not "simple", singularity structure and finite-size behavior.

The variation of $\mathcal{L}_L(T)$ with temperature (on a linear scale) is presented in Fig. 12 for the largest computationally feasible system-size of $N = 6400$ particles and, thus, of box size $L \simeq 18.6\sigma$. Note, first, that although $\mathcal{L}(T)$ rises sharply close to T_c, there seems to be a relatively large background contribution. If one chose to ignore this and merely examined a direct log-log plot extending over only one decade in ϵ, the resulting effective exponent would be of little theoretical significance. As shown by Sengers and coworkers,[15,16,57] the Onsager coefficient close to criticality may be written (in the thermodynamic limit, $L \to \infty$) as

$$\mathcal{L}(T) = \mathcal{L}_b(T) + \Delta\mathcal{L}(T), \tag{37}$$

where $\mathcal{L}_b(T)$ is a slowly varying background term which arises from fluctuations at small length scales, of order σ, while $\Delta\mathcal{L}(T)$ represents the "critical enhancement" induced by long-range fluctuations on the scale of the diverging correlation length $\xi(T) \sim \epsilon^{-\nu}$. The singular piece is predicted to diverge as

$$\Delta\mathcal{L}(T) \approx QT^*/\epsilon^{\nu_\lambda} \tag{38}$$

with an amplitude Q and an exponent

$$\nu_\lambda = x_\lambda \nu \simeq 0.567 \quad \text{with} \quad x_\lambda = 1 - \eta - x_\eta \,, \tag{39}$$

where x_η is defined via Eq. (28) and expresses the weak divergence of the viscosity $\eta(T)$, while $\eta \simeq 0.03$ is the standard critical exponent[59] [that enters the scaling relation $\gamma = (2-\eta)\nu$].

Furthermore, we may invoke the "extended Stokes-Einstein relation"[19,60]

$$\Delta D_{\rm AB}(T) \approx R_D k_{\rm B} T/6\pi\eta(T)\xi(T), \tag{40}$$

which embodies the relation $x_D = 1 + x_\eta$ [see (36) and Ref. 11]. This is expected to describe the singular part, $\Delta D_{\rm AB}$, of the mutual diffusion coefficient $D_{\rm AB}(T)$ and so leads to the explicit expression

$$Q = R_D \Gamma_0 \, \sigma/6\pi\eta_0\xi_0 \tag{41}$$

for the amplitude in (38). Here R_D is a universal constant of order unity while Γ_0, η_0, and ξ_0 are the critical amplitudes for χ^*, η^*, and ξ defined via Eqs. (14), (28) and (16).

Two theoretical methods have been developed to calculate the universal dynamic amplitude ratio R_D, namely, mode-coupling theory of critical dynamics and dynamic renormalization-group theory.[19] In first approximation, mode-coupling theory yields[13] $R_D = 1.00$; but when memory and nonlocal effects are included one obtains the improved estimate[61] $R_D = 1.03$. The early theoretical values obtained from renormalization-group theory have varied from 0.8 to 1.2 due to various approximations, as reviewed by Folk and Moser.[20] The calculation of Folk and Moser with the fewest approximations has yielded $R_D = 1.063$. Experiments give values consistent with the mode-coupling prediction.[57,62] Here we follow Luettmer-Strathmann *et al.*[15] and adopt the estimate $R_D = 1.05$ as a compromise between the predictions of mode-coupling theory and the renormalization-group calculations. Using the estimates reported above for the amplitudes in (41) then yields

$$Q = (2.8 \pm 0.4) \times 10^{-3} \tag{42}$$

as a numerical prediction for the present model.

Our aim now is to discover if this theoretical analysis and the value (42) for Q are consistent with the evidence available from our simulations. Because of the computational demands imposed by the collective transport properties we have obtained results over a substantial temperature range only for the ($N = 6400$)-particle system; however, for $T^* = 1.48 \simeq 1.04\ T_c^*$ we also computed $\mathcal{L}_L(T)$ for $N = 400$, 1600, and 3200.

To analyze these data we write the finite-size scaling ansatz as[39,42,58]

$$\Delta\mathcal{L}_L(T) = \mathcal{L}(T) - \mathcal{L}_b(T) \approx Q\, T^* W(y)/\epsilon^{\nu_\lambda}, \tag{43}$$

where $y = L/\xi$ while $W(y)$ is the finite-size scaling function. As already discussed in the context of static critical phenomena, one requires $W(y) \to 1$ when $y \to \infty$ so as to reproduce the correct behavior (38) in the thermodynamic limit. In this case, however, it is not clear how rapidly $W(y)$ should approach unity. Indeed, since transport properties are calculated from time correlation functions of currents, they reflect the nonequilibrium behavior of the system. Although the exponentially rapid approach that applies in the static case [see Eq. (17)] might still be realized here, the well known, noncritical long-time tails in the correlation functions, etc., suggest that a slower, power-law approach cannot be excluded.

On the other hand, for finite L all properties remain bounded through criticality so that in the limit $y \to 0$ one should have

$$W(y) \approx W_0 y^{x_\lambda}[1 + W_1 y^{1/\nu} + ...\ ], \tag{44}$$

as in (18), where from (39) we have $x_\lambda \simeq 0.90$.

Of course, we do not know the value of the background $\mathcal{L}_b(T)$ in (43); but since it is slowly varying, we may reasonably replace it by a constant effective value $\mathcal{L}_b^{eff}$. Then, by treating $\mathcal{L}_b^{eff}$ as an adjustable parameter and examining the simulation data for $\mathcal{W}_L(T) = \Delta\mathcal{L}_L(T)\epsilon^{\nu_\lambda}/T^*$ as T and L vary with ν_λ set to its Ising value, we may seek an optimal data collapse onto the scaling form $QW[L/\xi(T)]$. Note that if this is achieved, the value Q should emerge when $y = L/\xi$ becomes large.[58]

Fig. 13 presents separated plots of $\mathcal{W}_L(T)$ vs. $y/(y + y_0)$, with, as in Fig 3, $y_0 = 7$, for four assignments of $\mathcal{L}_b^{eff}$. Note that the filled symbols represent the data at $T^* = 1.48$ for system sizes $L/\sigma \simeq 7.37,\ 11.70,\ 14.74$, and 18.57; their reasonably good collapse onto the remaining data (all for $L/\sigma \simeq 18.57$) and their approach towards 0 for small y serve to

justify

$$\mathcal{L}_b^{eff} = (3.3 \pm 0.8) \times 10^{-3} \tag{45}$$

as a sensible estimate of the background term in the Onsager coefficient: compare with Fig. 12. The horizontal arrows marked on the right side of Fig. 13 indicate the central theoretical value (42) for the amplitude Q. It is evident that the agreement is surprisingly good. Indeed, had one been asked to estimate Q from these plots one might have proposed $Q = (2.7 \pm 0.4) \times 10^{-3}$, again surprisingly close to the theoretical value. Further details of this finite-size scaling analysis, including a fit for $\mathcal{W}_L(T)$, are presented in Ref. 58.

Thus we conclude that our simulation data are, in fact, fully consistent with the predictions of the theory including the value 0.567 for the exponent ν_λ, and, hence, the result $x_D \simeq 1.0679$ for the interdiffusion coefficient itself. It cannot be emphasized too strongly, however, that our discussion demonstrates that in the analysis of simulations near critical points one needs to account properly for the inevitable finite-size effects and, when theory indicates, also for appropriate background contributions typically arising from short-range fluctuations.[58]

VI. SUMMARY

We have studied the static and dynamic properties of a symmetric truncated Lennard-Jones binary fluid model with $\sigma_{\rm AA} = \sigma_{\rm BB} = \sigma_{\rm AB} = \sigma$, $\varepsilon_{\rm AA} = \varepsilon_{\rm BB} = 2\varepsilon_{\rm AB} = \varepsilon$ and masses $m_{\rm A} = m_{\rm B} = m$. This model has a liquid-liquid miscibility gap. We have used a combination of semi-grandcanonical Monte Carlo (SGMC) and microcanonical molecular dynamics simulations to study both the static and dynamic properties near the demixing critical point. The symmetry of the model sets the critical composition at $x_{\rm A} = x_{\rm B} = 1/2$. We have studied the system at the comparatively high liquid density $\rho^* = \rho\sigma^3 = 1$, in which region the gas-liquid and liquid-solid transitions are far from the temperature range of interest.

The critical temperature T_c has been determined quite accurately as $T_c^* \equiv k_{\rm B}T_c/\varepsilon = 1.4230 \pm 0.0005$ using a variety of techniques. Because of the short-range nature of the interactions one anticipates that demixing criticality in the model belongs to the three-dimensional Ising universality class. All our data for the static properties near the critical point strongly support that presumption.

We have also presented the first comprehensive study of the dynamic properties of a binary fluid near the critical point. We find evidence for a very weak divergence of the shear viscosity, $\eta(T)$, near the critical point in accord with expectations. The self-diffusion constant $D(T)$ remains finite at the critical point which is consistent with some earlier studies. We also find that the Stokes-Einstein relation remains a fairly good approximation even within 0.5% of T_c.

In contrast to the self-diffusion constant, the interdiffusion constant $D_{\rm AB}(T)$ vanishes rapidly when $T \to T_c$. Our analysis of the simulation data supports the various theoretical predictions for the critical exponents of all these quantities including the dynamic exponent relation[11,19,60] $x_D = 1+x_\eta$. But, even with an accurate knowledge of T_c and of the correlation length and concentration susceptibility, it proves essential to consider the finite-size effects and allow for background contributions arising from short-range fluctuations, in order to properly analyze the data for the interdiffusion coefficient.

Finally, however, we have not discussed the bulk viscosity, $\eta_B(T)$, which is expected to diverge much more rapidly than the shear viscosity.[21] That remains a significant task for future work.

Acknowledgement

M.E.F. and S.K.D. are grateful for support from the National Science Foundation under Grant No. CHE 03-01101. S.K.D. also acknowledges financial support from the Deutsche Forschungsgemeinschaft (DFG) via Grant No. Bi 314/18-2 and thanks Professor Kurt Binder and Dr. Jürgen Horbach for supporting his stay in the Johannes Gutenberg Universität Mainz, Germany, where all the simulations were carried out with their close collaboration.

[1] M.E. Fisher and G. Orkoulas, Phys. Rev. Lett. **85**, 696 (2000); G. Orkoulas, M.E. Fisher, and C. Üstün, J. Chem. Phys. **113**, 7530 (2000).

[2] A. Kostrowicka Wyczalkowska, J.V. Sengers, and M.A. Anisimov, Physica A **334**, 482 (2004); M.A. Anisimow and J.V. Sengers, in *Equations of State for Fluids and Fluid Mixtures*, edited by J.V. Sengers, R.F. Kayser, C.J. Peters, and H.J. White, Jr. (Elsevier, Amsterdam, 2000) p. 381.

[3] J. Zinn-Justin, Phys. Repts. **344**, 159 (2001).

[4] K. Binder and E. Luijten, Phys. Repts. **344**, 179 (2001).

[5] M. Hasenbusch, Int. J. Mod. Phys. C **12**, 911 (2001).

[6] A. Pelissetto and E. Vicari, Phys. Repts. **368**, 549 (2002).

[7] N.B. Wilding, J. Phys.: Condens. Matter **9**, 585 (1997).

[8] E. Luijten, M.E. Fisher, and A.Z. Panagiotopoulos, Phys. Rev. Lett. **88**, 185701 (2002).

[9] (a) Y.C. Kim, M.E. Fisher, and E. Luijten, Phys. Rev. Lett. **91**, 065701 (2003); Y.C. Kim and M.E. Fisher, (b) Phys. Rev. E **68**, 041506 (2003); (c) Phys. Rev. Lett. **92**, 185703 (2004); (d) Computer Phys. Commun. **169**, 295 (2005).

[10] R.L.C. Vink and J. Horbach, J. Chem. Phys. **121**, 3253 (2004); J. Phys.: Condens. Matter **16**, S3807 (2004); R.L.C. Vink, J. Horbach and K. Binder, Phys. Rev. E **71**, 011401 (2005); R.L.C. Vink, preprint.

[11] H.C. Burstyn and J.V. Sengers, Phys. Rev. Lett. **45**, 259 (1980); Phys. Rev. A **25**, 448 (1982).

[12] L.P. Kadanoff and J. Swift, Phys. Rev. **166**, 89 (1968).

[13] K. Kawasaki, Ann. Phys. (N.Y.) **61**, 1 (1970); Phys. Rev. A **1**, 1750 (1970); A. Onuki, Phys. Rev. E **55**, 403 (1997).

[14] L. Mistura, Nuovo Cimento **12**B, 35 (1972); J. Chem. Phys. **62**, 4571 (1975).

[15] J. Luettmer-Strathmann, J.V. Sengers, and G.A. Olchowy, J. Chem. Phys. **103**, 7482 (1995).

[16] J. Luettmer-Strathmann and J.V. Sengers, J. Chem. Phys. **104**, 3028 (1996).

[17] K. Kawasaki, in *Phase Transitions and Critical Phenomena*, Vol. 5A, edited by C. Domb and M.S. Green (Academic, New York, 1976), p. 165.

[18] E.D. Siggia, B.I. Halperin and P.C. Hohenberg, Phys. Rev. B **13**, 2110 (1976).

[19] P.C. Hohenberg and B.I. Halperin, Rev. Mod. Phys. **49**, 435 (1977).

[20] R. Folk and G. Moser, Phys. Rev. Lett. **75**, 2706 (1995).

[21] A. Onuki, *Phase Transition Dynamics* (Cambridge Univ. Press, Cambridge, U.K., 2002).

[22] T. Hamanaka, R. Yamamoto and A. Onuki, Phys. Rev. E **71**, 011507 (2005).

[23] A. Chen, E.H. Chimowitz, S. De, and Y. Shapir, Phys. Rev. Lett. **95**, 255701 (2005). These authors found results for thermal equilibration at criticality that were consistent with theoretical predictions; but they noticed the large discrepency with the conclusions of JY (Ref. 24) and expressed the hope that future investigations would clarify the issue. We believe our work does that.

[24] K. Jagannathan and A. Yethiraj, Phys. Rev. Lett. **93**, 015701 (2004); J. Chem. Phys. **122**, 244506 (2005); Phys. Rev. Lett. **94**, 069602 (2005).

[25] B. Widom and J.S. Rowlinson, J. Chem. Phys. **15**, 1670 (1970).

[26] J.V. Sengers and M.R. Moldover, Phys. Rev. Lett. **94**, 069601 (2005).

[27] S.K. Das, J. Horbach, and K. Binder, J. Chem. Phys. **119**, 1547 (2003)

[28] S.K. Das, J. Horbach, and K. Binder, Phase Transitions **77**, 823 (2004).

[29] K. Binder, S.K. Das, J. Horbach, M. Müller, R.L.C. Vink, and P. Virnau, in *Multiscale Modelling and Simulation*, edited by S. Attinger and P. Koumoutsakos (Springer, Berlin, 2004) p. 169.

[30] K. Binder, Phys. Rev. Lett. **45**, 811 (1980); Z. Phys. B**45**, 61 (1981); K. Binder, J.L. Lebowitz, M.K. Phani and M.H. Kalos, Acta Metall. **29**, 1655 (1981).

[31] J.G. Briano and E.D. Glandt, J. Chem. Phys. **80**, 3336 (1984); D.A. Kofke and E.D. Glandt, Fluid Phase Equilibria **29**, 327 (1986).

[32] A. Sariban and K. Binder, J. Chem. Phys. **86**, 5859 (1987); H.-P. Deutsch and K. Binder, Macromolecules **25**, 6214 (1992).

[33] E. de Miguel, E. Martin del Rio, and M.M. Telo da Gama, J. Chem. Phys. **103**, 6188 (1995).

[34] D.P. Landau and K. Binder, *A Guide to Monte Carlo Simulations in Statistical Physics*, 2nd ed. (Cambridge Univ. Press, Cambridge, 2005).

[35] M.P. Allen and D.J. Tildesley, *Computer Simulations of Liquids* (Clarendon Press, Oxford, 1987).

[36] D.C. Rapaport, *The Art of Molecular Dynamics Simulation* (Cambridge Univ. Press, Cambridge, U.K., 1995).

[37] K. Binder and G. Ciccotti (eds.) *Monte Carlo and Molecular Dynamics of Condensed Matter Systems* (Italian Physical Society, Bologna, 1996).

[38] D. Frenkel and B. Smit, *Understanding Molecular Simulation: From Algorithms to Applications*, second ed. (Academic Press, New York, 2002).

[39] M.E. Fisher, in *Critical Phenomena*, edited by M.S. Green (Academic Press, London, 1971) p. 1.

[40] K. Binder, in *Computational Methods in Field Theory*, edited by C.B. Lang and H. Gausterer (Springer, Berlin, 1992) p. 59.

[41] M.N. Barber, in *Phase Transition and Critical Phenomena, Vol. 8*, edited by C. Domb and J.L. Lebowitz (Academic Press, New York, 1983) p. 145.

[42] V. Privman (ed.) *Finite Size Scaling and Numerical Simulation of Statistical Systems* (World Scientific, Singapore, 1990).

[43] Depending upon the proximity to the critical point, average was taken over 10 to 15 distinct initial configurations.

[44] K. Binder, Z. Phys. B **43**, 119 (1981).

[45] Y.C. Kim, M.E. Fisher and A.Z. Panagiotopoulos, Phys. Rev. Lett. **95**, 195703 (2005).

[46] Y.C. Kim and M.E. Fisher, J. Phys. Chem. B **108**, 6750 (2004).

[47] A.B. Bhatia and D.E. Thornton, Phys. Rev. B **52**, 3004 (1970).

[48] Note that the calculation of the mean square displacements was not subject to periodic boundary conditions, so they can grow without limit.

[49] R. Kutner, K. Binder and K.W. Kehr, Phys. Rev. B **26**, 2967 (1982).

[50] M.W. Maddock, G. Goodyear, and S.C. Tucker, J. Phys. Chem. B **104**, 6266 (2000); A.N. Drozdov and S.C. Tucker, J. Chem. Phys. **114**, 4912 (2001); J. Phys. Chem. B**105**, 6675 (2001); J. Chem. Phys. **116**, 6381 (2002).

[51] K.R. Harris, J. Chem. Phys. **116**, 6379 (2002).

[52] J.-P. Hansen and I.R. McDonald, *Theory of Simple Liquids* (Academic, London, 1986).

[53] R.A. Ferrell and J.K. Bhattacharjee, Phys. Rev. A **31**, 1788 (1985); J.K. Bhattacharjee and R.A. Ferrell, Physica (Amsterdam) **250A**, 83 (1998); H. Hao, R.A. Ferrell, and J.K. Bhattacharjee, Phys. Rev. E **71**, 021201 (2005).

[54] R.F. Berg, M.R. Moldover, and G.A. Zimmerli, Phys. Rev. Lett. **82**, 920 (1999); Phys. Rev. E **60**, 4079 (1999).

[55] R.F. Berg and M.R. Moldover, J. Chem. Phys. **89**, 3694 (1988); Phys. Rev. A **42**, 7183 (1990); J. Chem. Phys. **93**, 1926 (1990); D. Madej and T. Hornowski, J. Phys. Condens. Matter **14**,

13429 (2002).

[56] J.V. Sengers and P.H. Keyes, Phys. Rev. Lett. **26**, 70 (1971).

[57] J.V. Sengers, Int. J. Thermophys. **6**, 203 (1985).

[58] S.K. Das, M.E. Fisher, J.V. Sengers, J. Horbach, and K. Binder, to be submitted.

[59] M.E. Fisher, Rev. Mod. Phys. **46**, 597 (1974).

[60] H.C. Burstyn, J.V. Sengers, and P. Esfandiari, Phys. Rev. A **22**, 282 (1980).

[61] H.C. Burstyn, J.V. Sengers, J.K. Bhattacharjee, and R.A. Ferrell, Phys. Rev. A **28**, 1567 (1983).

[62] R.A. Wilkinson, G.A. Zimmerli, H. Hao, M.R. Moldover, R.F. Berg, W.L. Johnson, R.A. Ferrell, and R.W. Gammon, Phys. Rev. E **57**, 436 (1998).

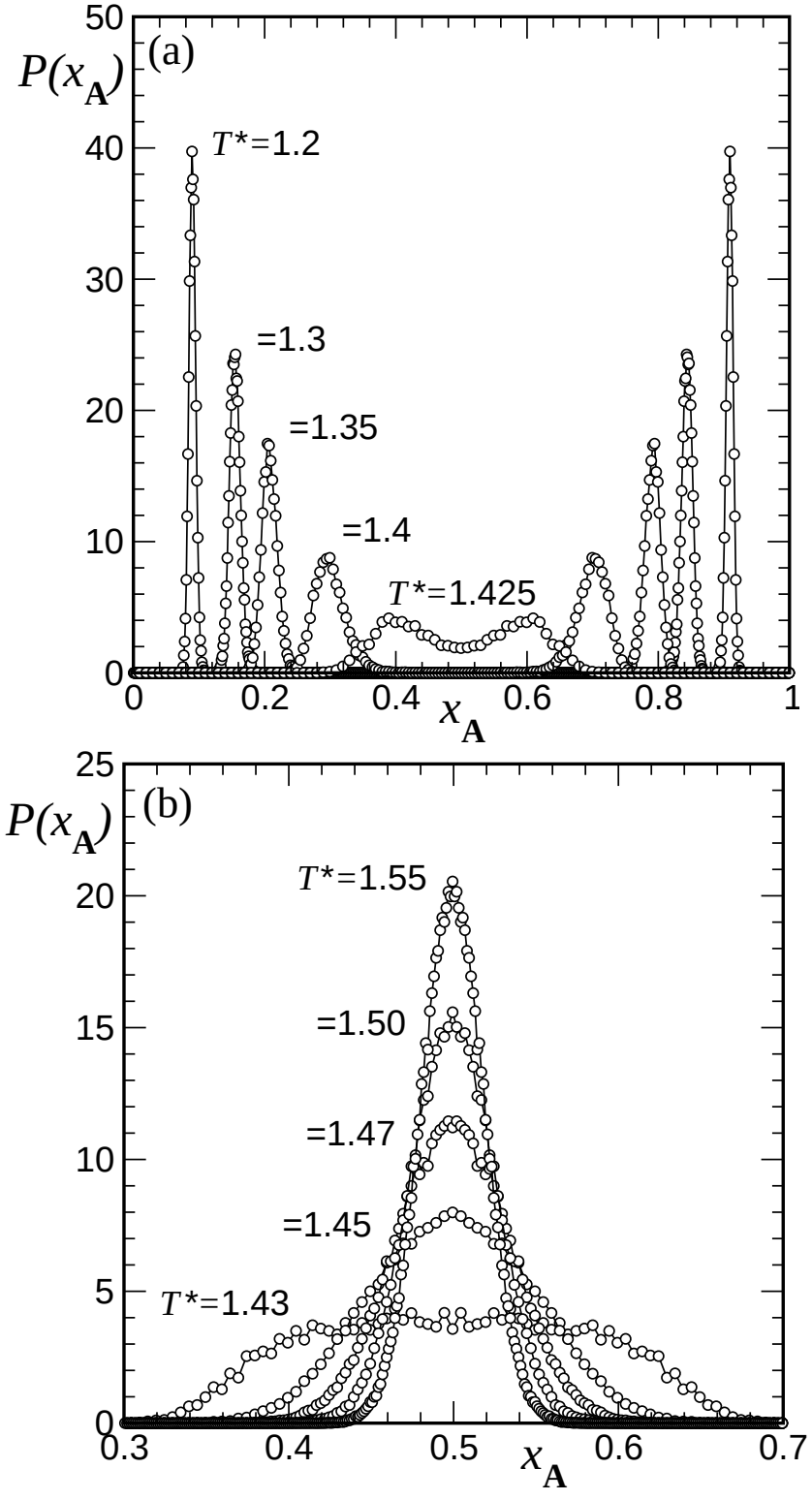

FIG. 1: Probability distributions $P(x_{\rm A})$ of the relative concentration $x_{\rm A} = N_{\rm A}/N$ of A particles for $N = 6400$ and chemical potential difference $\Delta\mu = 0$ at several temperatures (a) below T_c and (b) above T_c, respectively. For clarity many independent data points have been omitted.

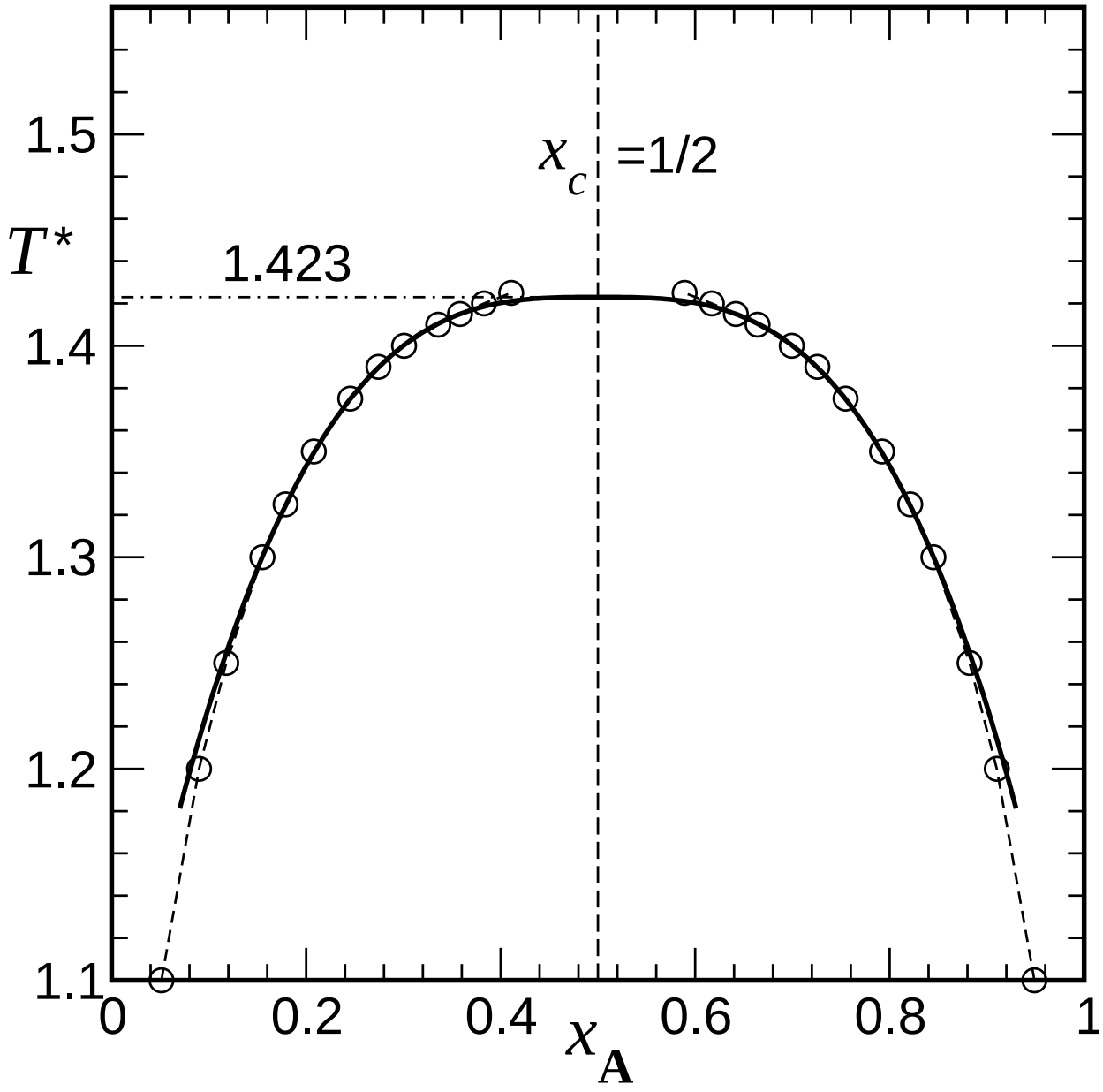

FIG. 2: Coexistence curve of the symmetrical (truncated) Lennard-Jones binary fluid in the plane of temperature T and concentration $x_{\rm A} = N_{\rm A}/N$, for overall density $\rho^* = 1.0$, the precise choice of potentials being given in Eqs. (1)-(4). Open circles are the simulation results for a system of $N = 6400$ particles, while the broken curve is only a guide to the eye. The solid curve indicates a fit to Eq. (13) which yields $T_c^* = 1.423$ as highlighted by the horizontal dot-dashed line.

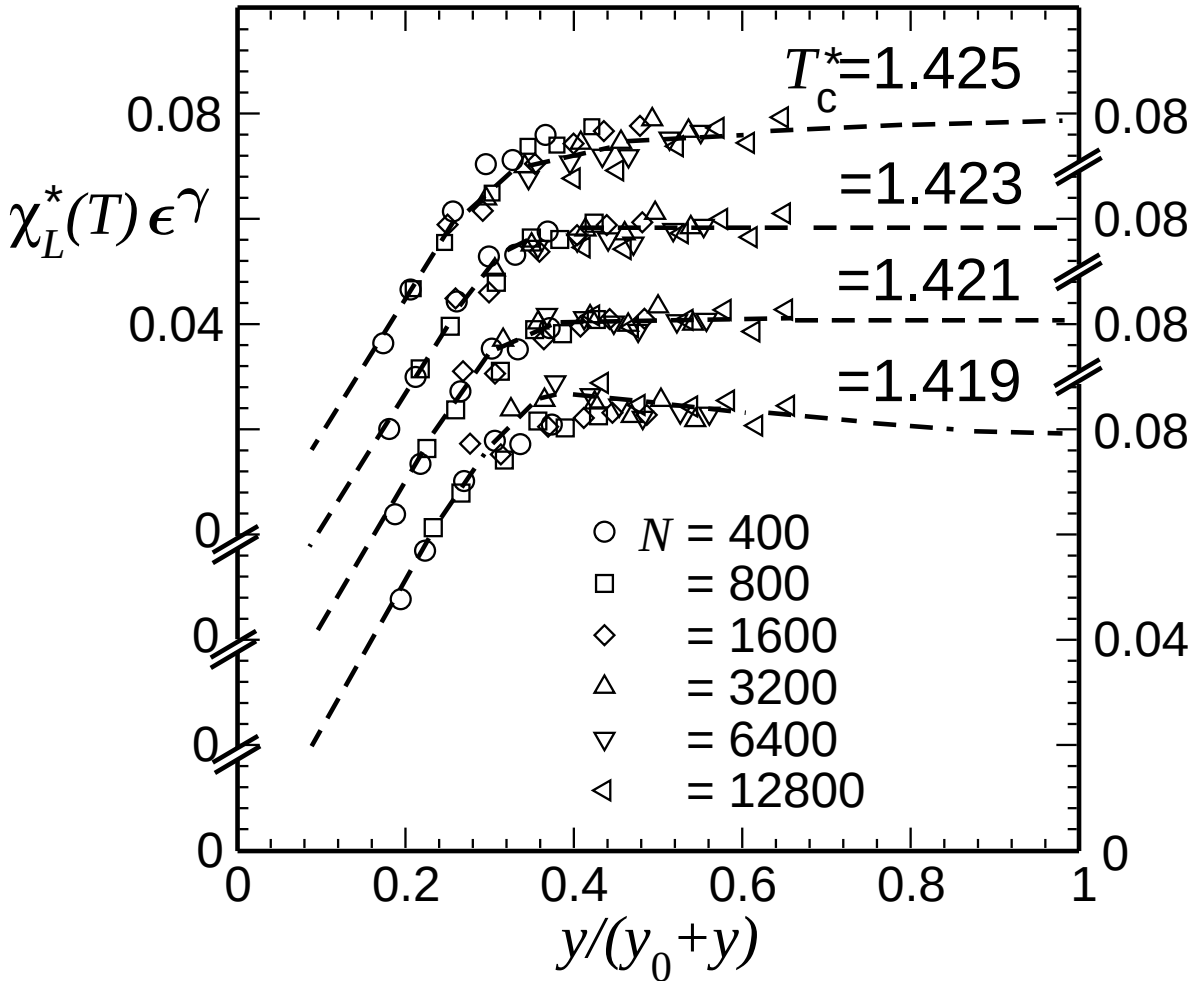

FIG. 3: Finite-size scaling plots of the susceptibility χ^* for temperatures above T_c using the trial values of T_c^* marked in the figure. The Ising values $\gamma = 1.239$, $\nu = 0.629$, have been accepted and simulation results for χ^* at temperatures $T^* = 1.45, 1.46, 1.48, 1.50, 1.52,$ and 1.55, are presented. Particle numbers from $N = 400$ to $N = 12800$ are included, as indicated (while the linear dimensions of the simulation box are $L = N^{1/3}\sigma$). The dashed lines are guides to the eye: in light of the degree of data collapse and the expected scaling function behavior stated in Eq. (17), the estimates $T_c^* = 1.423$ and 1.421 are quite acceptable.

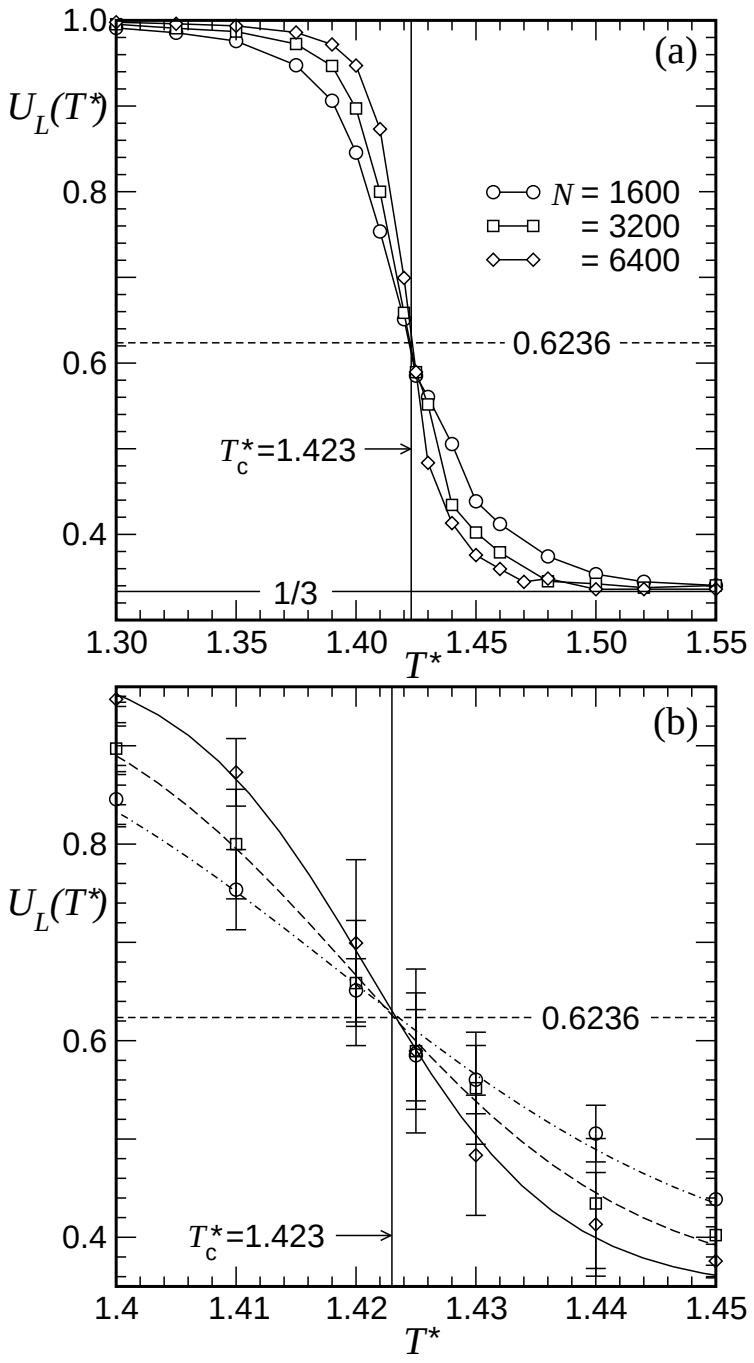

FIG. 4: The fourth-order cumulant $U_L(T)$ plotted vs. T for several system sizes, as indicated in the figure. The broken horizontal line indicates the value of the U_L at T_c for Ising type systems. The vertical line at $T^* = 1.423$ represents our preferred estimate of T_c^*. The smooth curves in the enlarged plot (b) are fits to tanh functions.

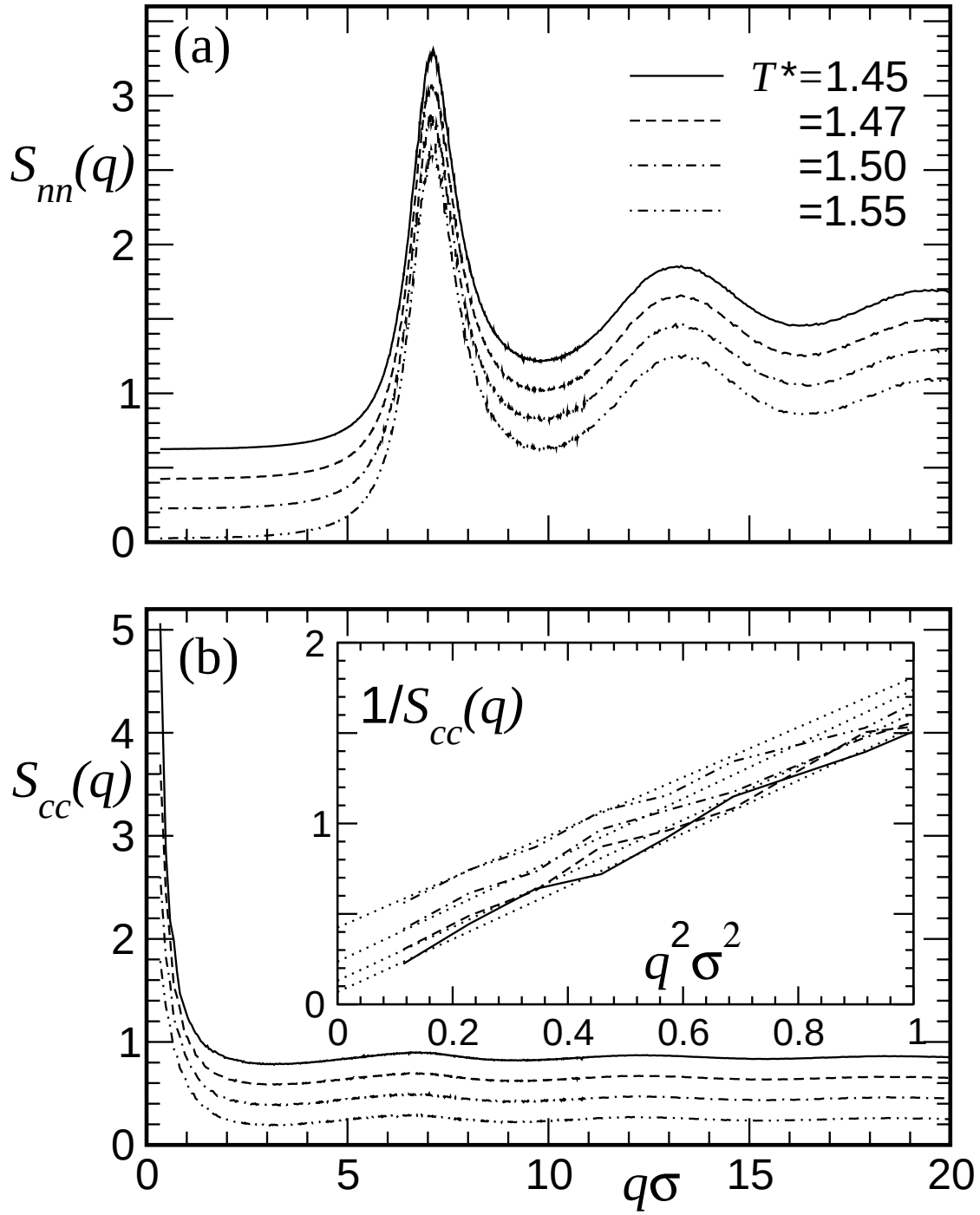

FIG. 5: Plot of the structure factors (a) $S_{nn}(q)$, (b) $S_{cc}(q)$, for various temperatures, versus momentum q. The various curves are shifted up by 0.2 relative to one another for clarity. All data refer to a system of $N = 6400$ particles. Inset in part (b) represents an Ornstein-Zernike plot which yields estimates for $\xi(T)$ via Eq. (22).

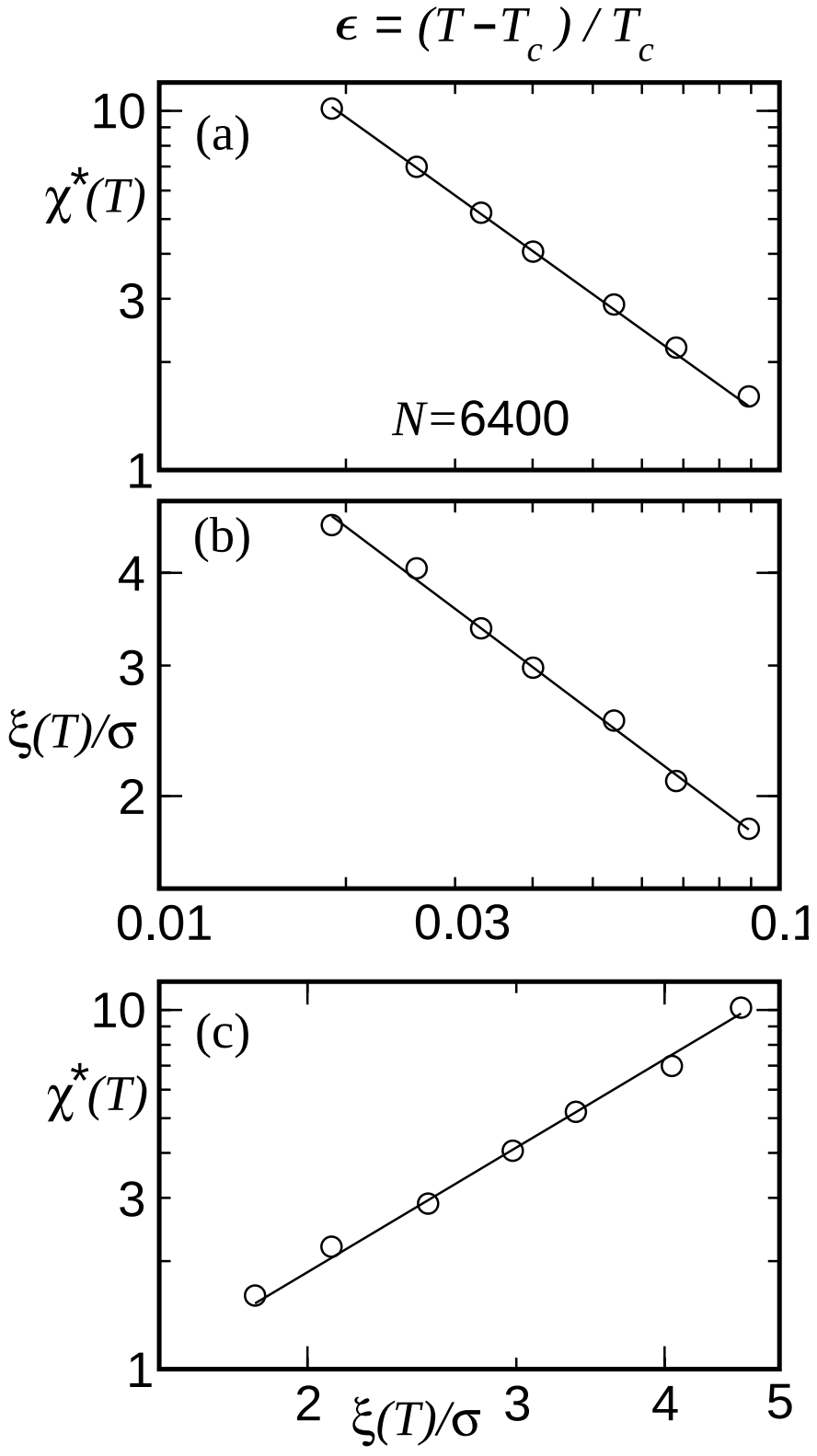

FIG. 6: Plots of (a) the reduced susceptibility χ^* and (b) the correlation length ξ versus ϵ. Part (c) shows the variation of χ with ξ. The lines represent fits using the anticipated Ising exponents. All the data refer to systems of $N = 6400$ particles.

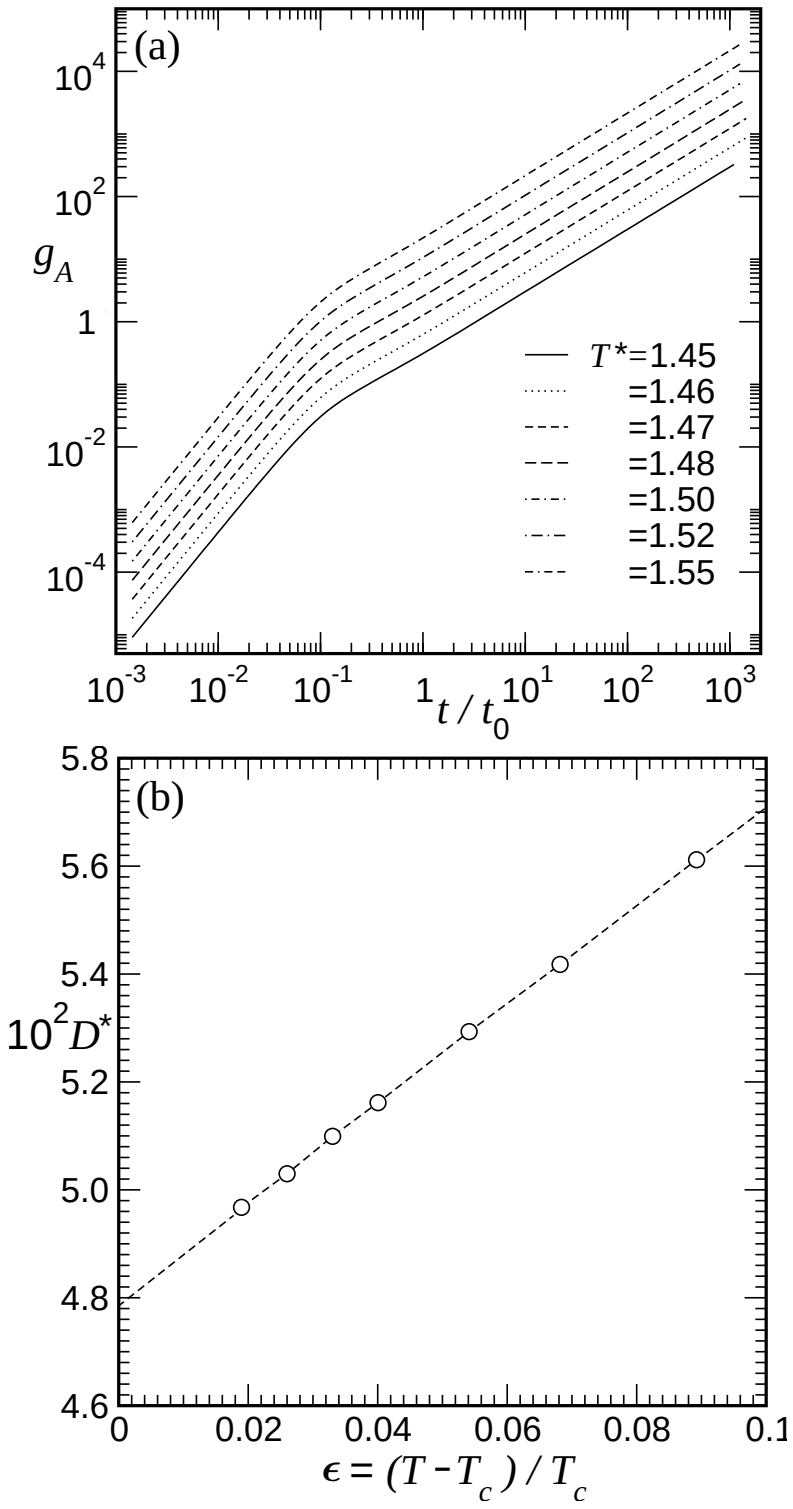

FIG. 7: (a) Log-log plot of the mean square displacements of all the particles versus time with $t_0 = (m\sigma^2/\varepsilon)^{1/2}$, for systems containing $N = 6400$ particles, at the critical concentration and the seven temperatures indicated. The plots for different T are displaced by factors of 2. (b) Variation of the reduced self-diffusion constant D^* with temperature.

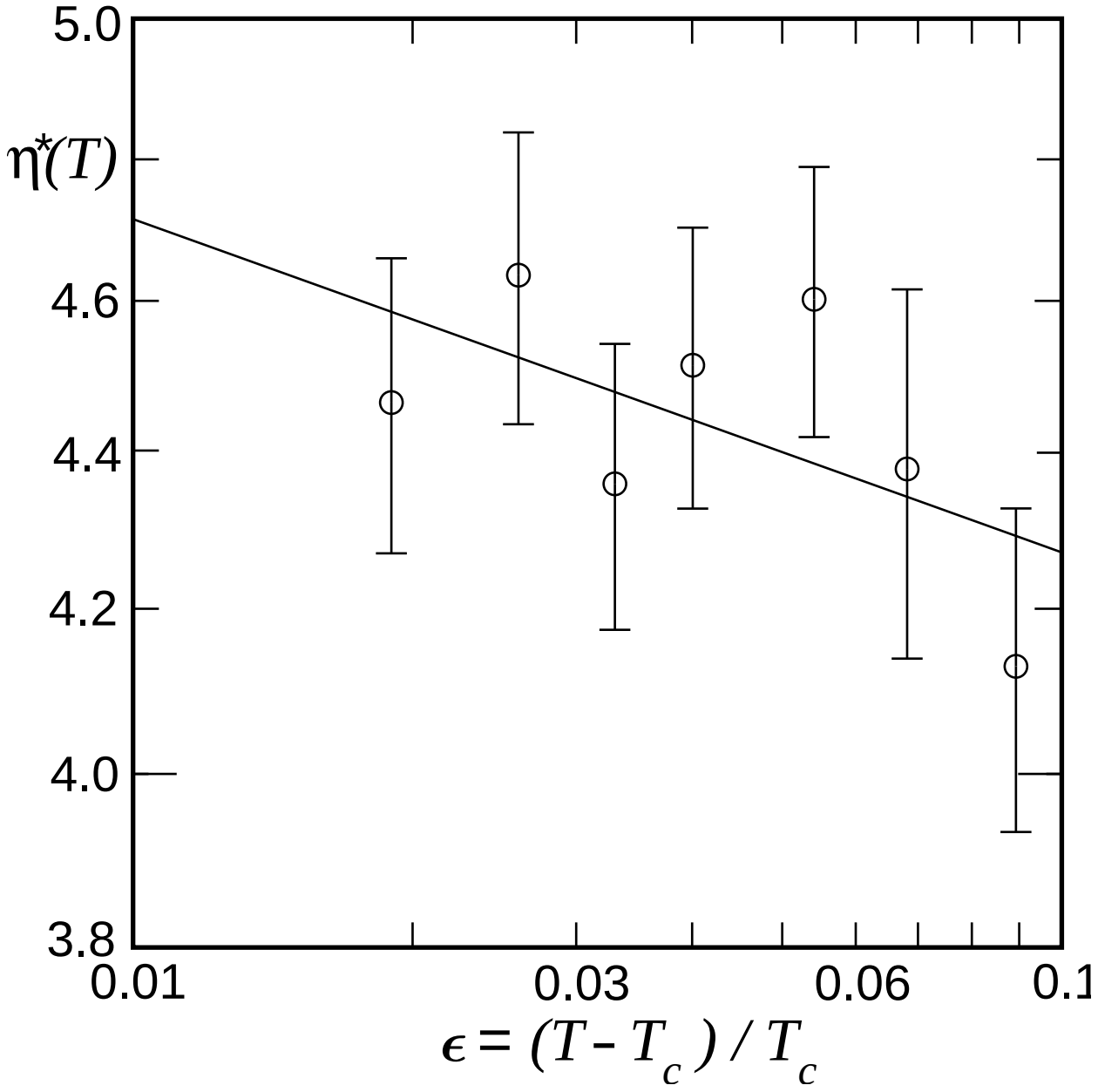

FIG. 8: A log-log plot of the reduced shear viscosity η^* vs. temperature. The line represents a least squares fit to the theoretical form (28) with $x_\eta = 0.068$ and $\nu = 0.629$, yielding an amplitude $\eta_0 = 3.8_7 \pm 0.3$.

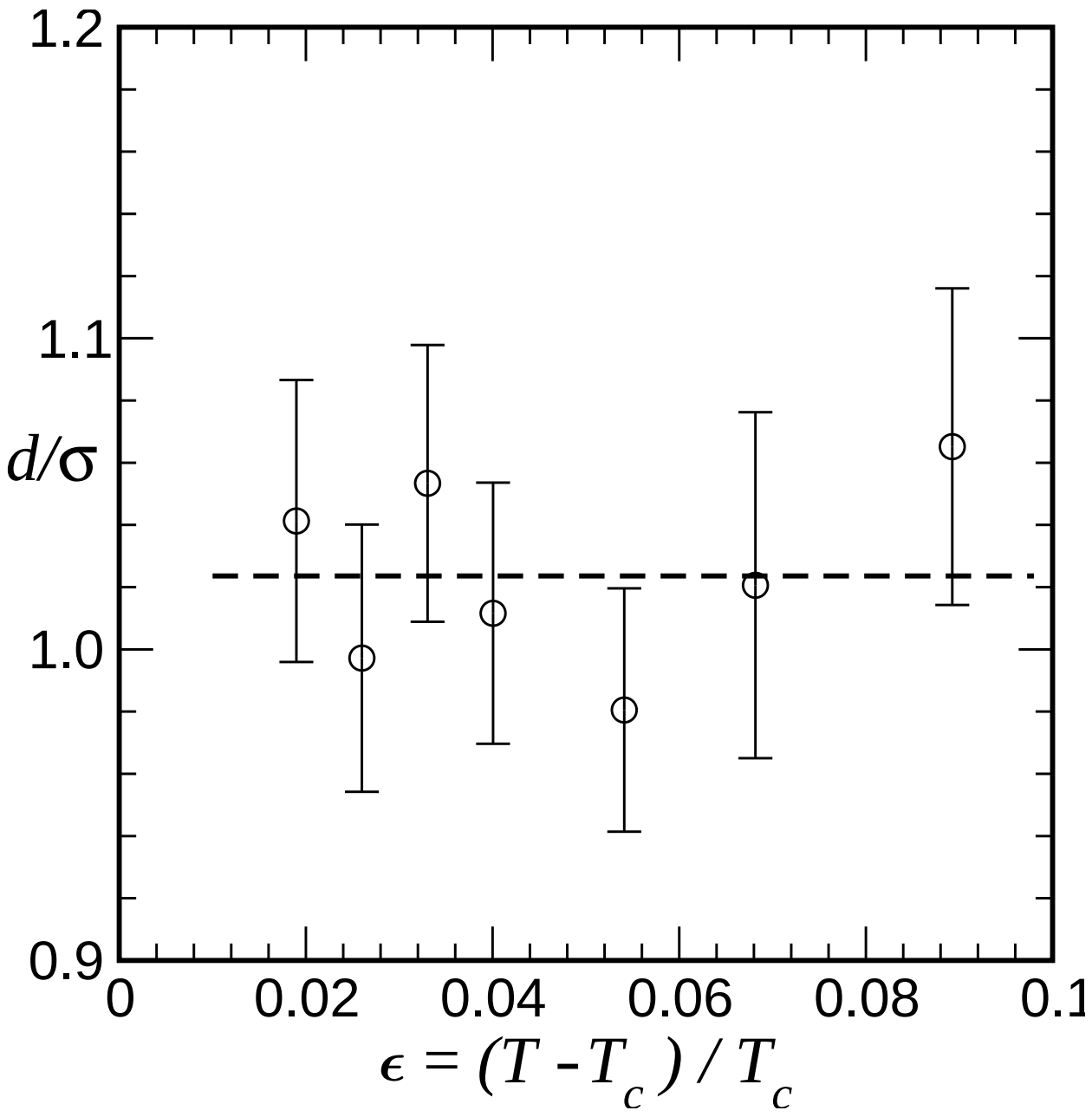

FIG. 9: Plot of the Stokes-Einstein diameter, d, as defined in Eq. (29), vs. temperature. The dashed line serves as a guide to the eye.

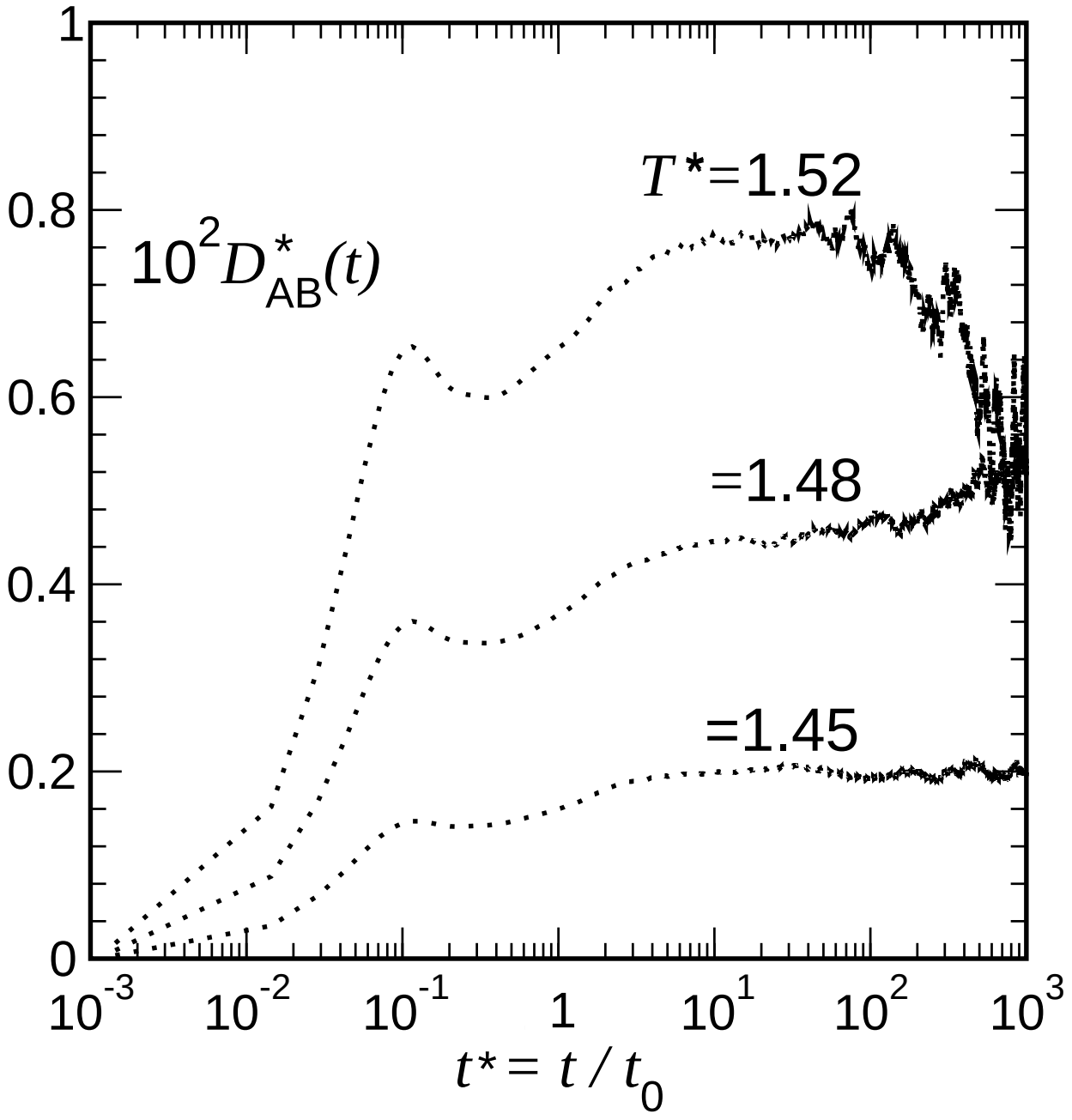

FIG. 10: Plot of the interdiffusion coefficient $D^*_{\rm AB}(t)$ vs. time at three different temperatures for systems of $N = 6400$ particles. The knees visible at short time are due to discrete integration time step Δt^*.

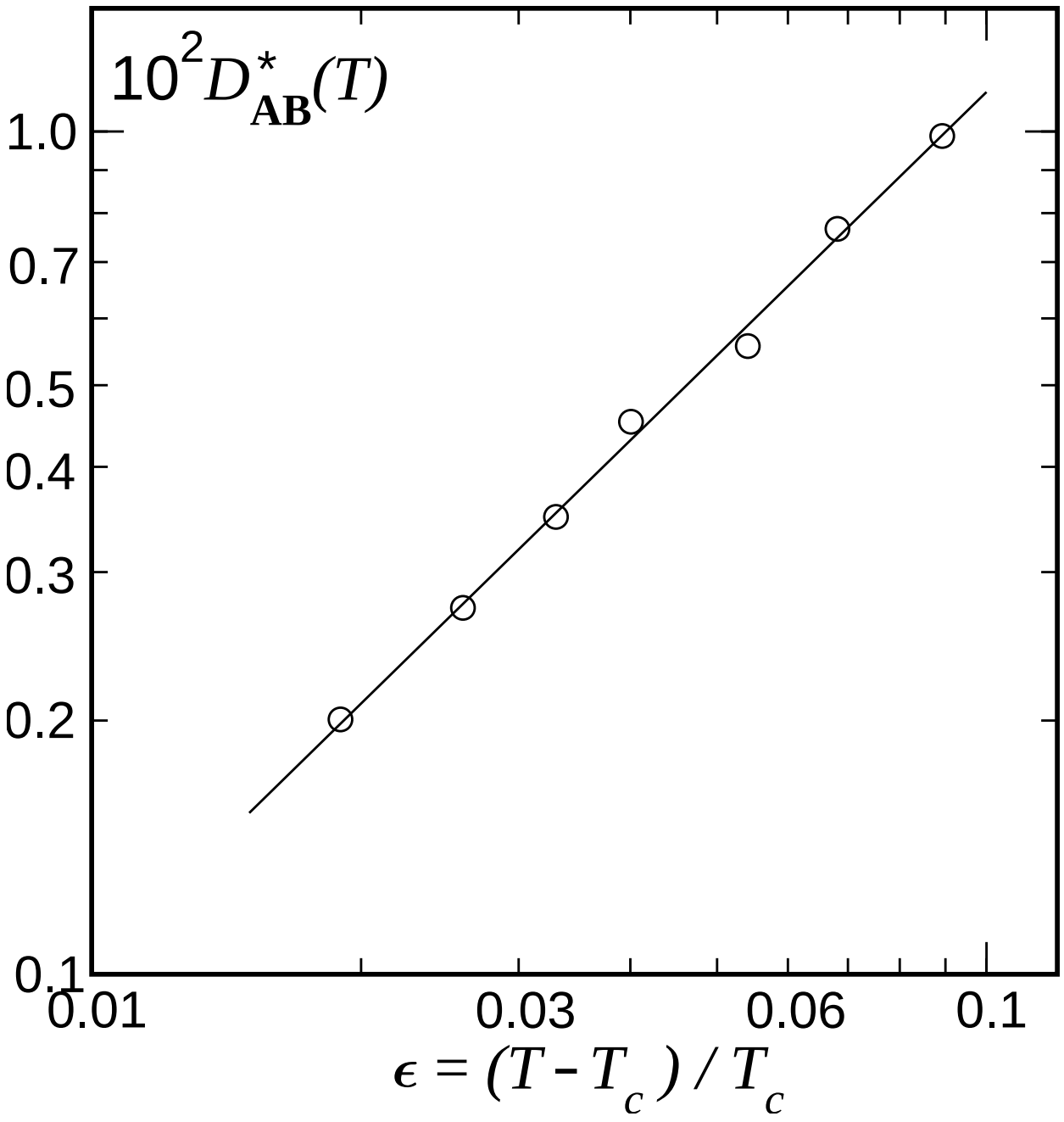

FIG. 11: Log-log plot of the interdiffusion coefficient $D^*_{\rm AB}$ as calculated vs. T. The line is a fit to the power law $D_{\rm AB} \sim \epsilon^{x_{\rm eff}\nu}$ which yields $x_{\rm eff} \simeq 1.6$. The data correspond to $N = 6400$.

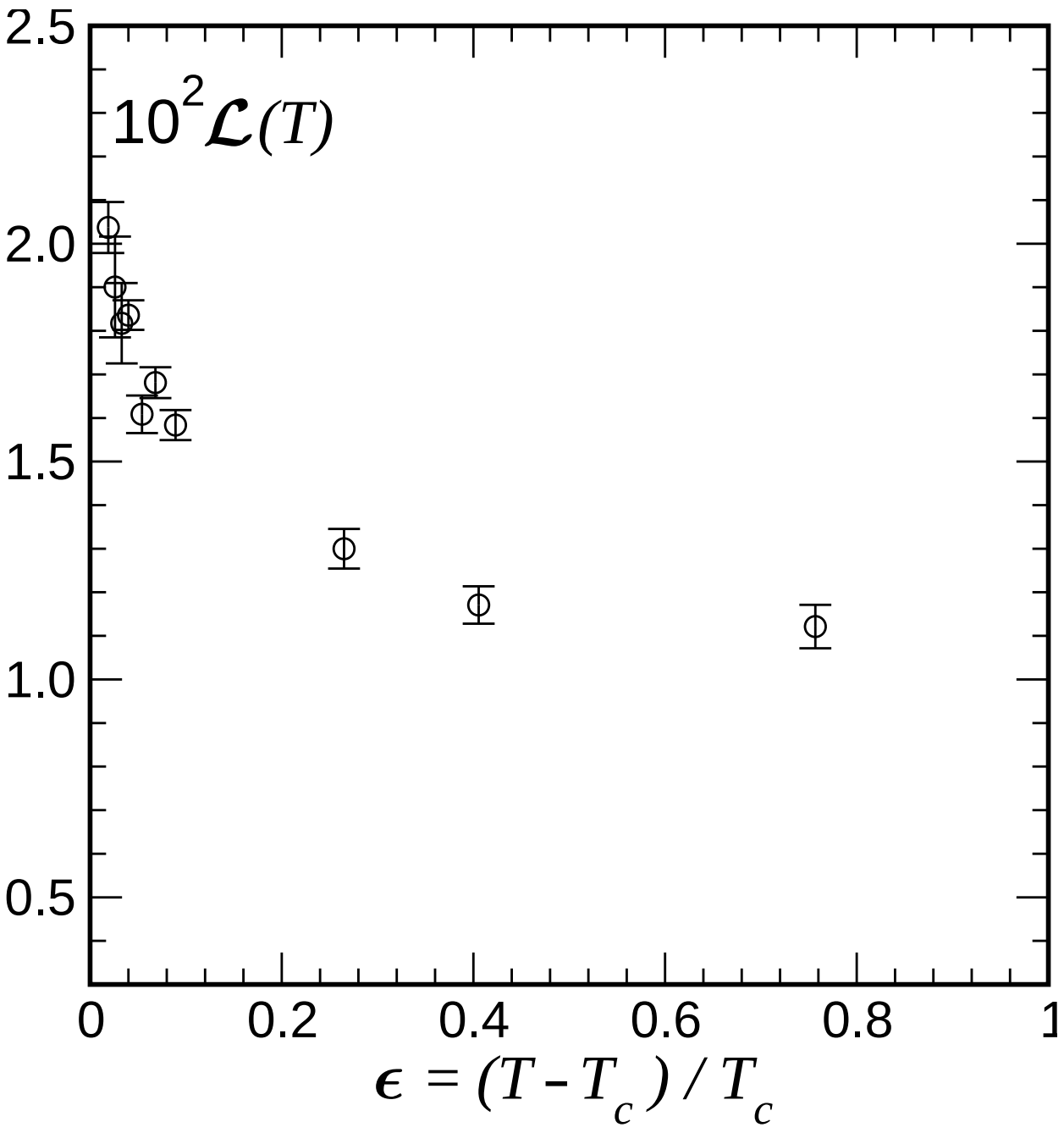

FIG. 12: Plot of the reduced Onsager coefficient $\mathcal{L}(T)$ vs. T for a system of $N = 6400$ particles. Note the "background" contribution and the sharp rise as T_c is approached. The four highest data points span the range from 1.9% to 4% above T_c; but the experiments[11] probe the range $\epsilon = 10^{-1}$ to 10^{-4}.

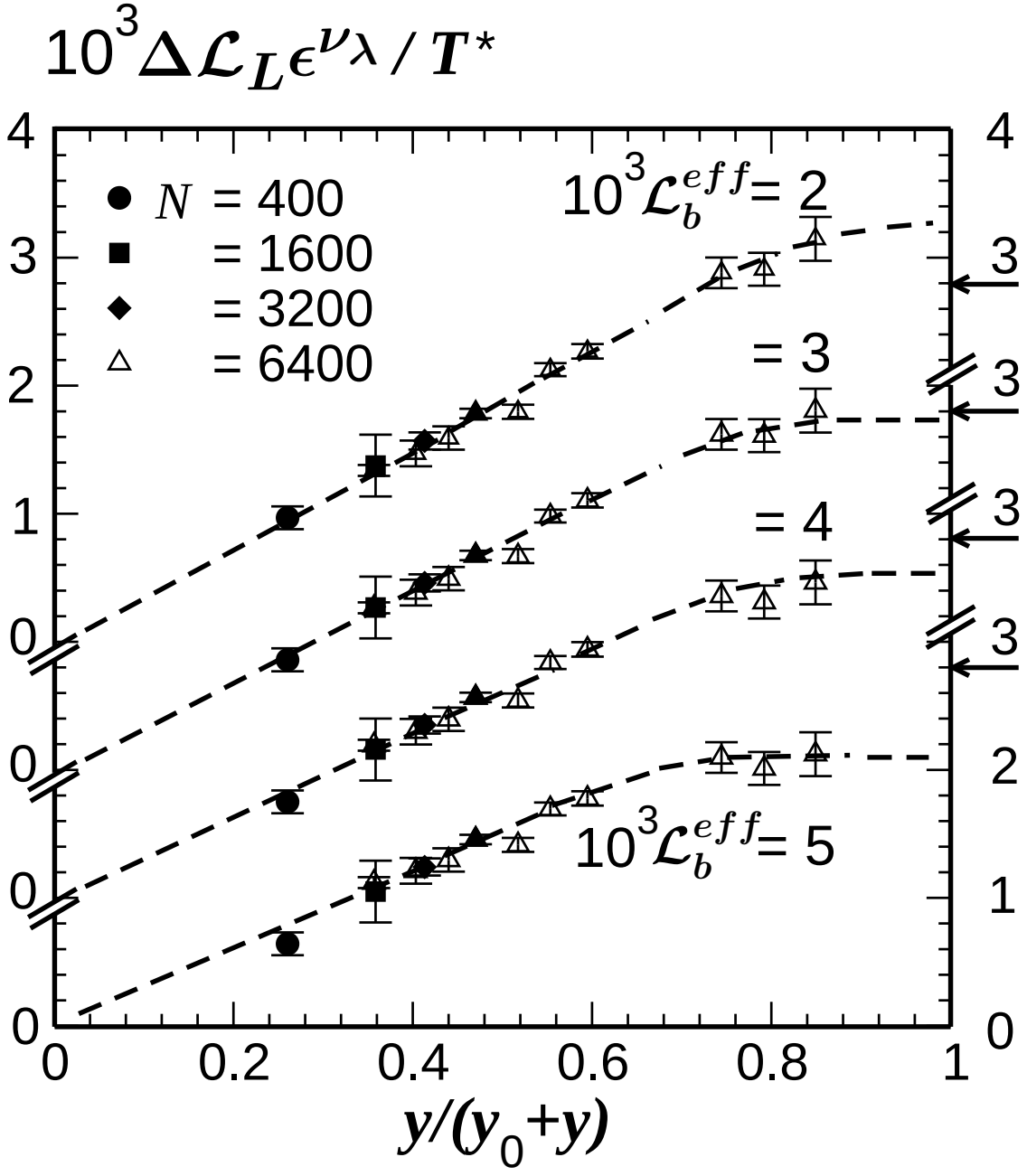

FIG. 13: Finite-size scaling plots for the interdiffusional Onsager coefficient $\mathcal{L}_L(T)$ with $\epsilon = (T - T_c)/T_c$, $y = L/\xi(T)$, and trial values for the effective background contribution $\mathcal{L}_b^{eff}$. The approximate Ising value $\nu_\lambda = 0.567$ has been adopted and, for convenience, we have set $y_0 = 7$ in the abscissa variable, $y/(y_0 + y)$, that approaches unity when $L \to \infty$. The filled symbols represent data at $\epsilon \simeq 4.0 \times 10^{-2}$ for different system sizes of $N = 400$ to 6400 particles and fixed density $\rho\sigma^3 = 1$. The solid arrows on the right hand axis indicate the central theoretical estimate for the critical amplitude Q: see text.